CHAPTER 1

INTRODUCTION

1.1 Thermoelectric Materials

Large and continuous requirement of energy resulted in attraction of scientist and researchers towards efficient and alternate technologies which can reduce ozone layer depletion, greenhouse gas discharge, and fossil fuel usage. Thermoelectric materials are adept to transform electricity into thermal energy for purpose of cooling , heating or it can transform waste heat and convert it to electricity, are seen as viable and efficient option to reduce carbon and greenhouse gas discharge and provide clean and nature friendly forms of energy. Thermoelectric materials are basically semiconductor materials which are most suitable for fabrications of ICs and devices [1].

Thermoelectric materials has the capability to completely reform thermal heating ,thermal cooling and electrical power formation by cogently strengthening efficiency of ongoing methods and hence decreases reliance upon natural energy sources. Present coal, gas, and nuke power generation processes are typically only 40% efficient and it is proposed that if a further 1% of their primary energy could be recovered,approximately 200 TW of electricity may be produced yearly within the EU, with a significant associated reductions in CO_2 emissions.However, increasing thermoelectric efficiency of present materials is a major hindrance to larger acceptance of this latest technology.[2]

In past decade, there had been deepen interest in area of thermoelectrics, motivated by the requirement of highly efficient materials for refrigeration and electricity production.Some research efforts are mainly concentrated on reducing thermal conductivity contributed by lattice and rest research efforts focus upon materials that shows large power factors.Proposed energy efficient application of thermoelectric compound are responsible for enhanced activity in this field by creating demand of extra efficient thermoelectric materials in comparison to those which are presently in use.[3]

In an effort to minimize humans reliance upon natural resources for power production there is requirement of alternative way by virtue of which we can save fuel and cause smaller amount of damage to environment. Popular possible way is high temperature energy harvesting which involves direct recovery of unused heat energy and converting it to electricity.

Thermoelectric material efficiency is estimated by the dimensionless qauntity which is denoted by symbol ZT i.e. figure of merit which is obtained by formula given below:

$$\mathbf{ZT} = \frac{\boldsymbol{S^2 \sigma T}}{\boldsymbol{K}} \qquad (1.1)$$

where , 'T' is temperature,' S' is Seebeck coefficient,'σ' is electrical conductivity & 'K' is thermal conductivity which is the addition of electronic thermal (K_e) & lattice thermal (K_L) conductivities.[4]

In this project work our main aim is to improve the value of ZT of the Bismuth Telluride(Bi_2Te_3) which is a thermoelectric materials.Bismuth telluride, Bi_2Te_3, was reported for first time as an effective TE material in 1954 [5].Its unit cell is rhombohedral, although bismuth telluride crystal structure can be also expressed in term of a hexagonal unit cell [5]. The single crystal of Bi_2Te_3 is anisotropic. It is such that Bi and Te atoms are grouped and arranged in parallel layers which are stacked within a unit cell in the direction following the sequence: [5]

– Te(1) – Bi – Te(2) – Bi – Te(1) –

Above shown sequence is regularly repeated. There exist two different types of bonding between the Bi and Te atoms. Atoms of Bi are actively bound to Te atoms via covalent-ionic bond on both types of site, but the layers of Te(1) atoms are weakly bound by van der Waal's force to neighbouring tellurium layers [5]

Bismuth telluride is semiconductor compound .It is when mixed with selenium or antimony, it behaves as a proficient thermoelectric material suitable for portable power generation or refrigeration. It is a small band gap semiconductor with trigonal unit cell. It is produced by sealing bismuth and tellurium metals in a quartz tube under vacuum.[6]Bismuth telluride finds applications in the following:

- Electricity generation or cooling applications
- Topological insulators.

1.2 THERMOELECTRIC EFFECTS

In thermoelectric effect temperature gradient is basically used for generation of electricity by creating electric potential and vice versa.This effect is popularly used for production of electricity, temperature measurement or for fluctuating temperature of objects. Since in case of thermoelectric material (TE) the polarity of applied voltage is completely responsible for direction of cooling and heating.Probable application of TE devices is temperature controllers [7].

"Thermoelectric effect" consist of three separate effects:

- Seebeck effect
- Peltier effect
- Thomson effect

1.2.1 Seebeck effect

Seebeck observed that a circuit constructed from two different metals, with their junctions kept at divergent temperatures would create deflection in a compass magnet [8].Seebeck in the beginning assumed that it was because of magnetic induction due to temperature difference and thought it might be related with the magnetic field of earth. However, it was sooner accomplished that "Thermoelectric Force" generated electrical current, which according to Ampere's law magnet generates deflection in metal. The

temperature gradient generates electric potential (voltage) which can cause flow of electric current in closed circuit.

The voltage generated is directly dependent on temperature gradient between two junctions. The proportionality constant (S) is called **Seebeck's coefficient**, and often referred to as "thermopower" even though it is more related to potential than power. [9]

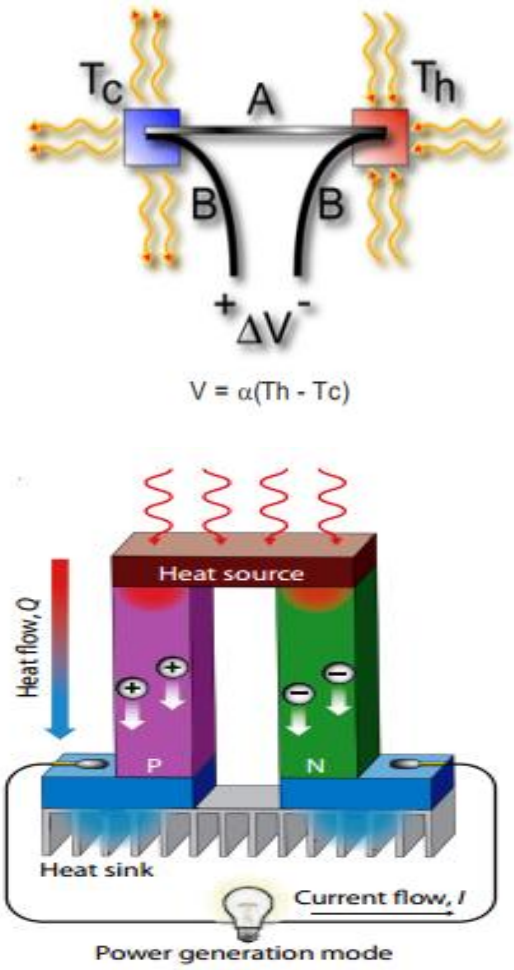

Figure 1.1 Seebeck Effect

Voltage difference(V) generated between terminals of an open circuit built from a pair of different metals, A and B, pair of junction is kept at different temperature, is completely dependent on the variation of temperature between the hot and cold junction T_h-T_c [10].

1.2.2 Peltier effect

In 1834,Peltier established that drift of current in a junction constructed from two different material create heating or cooling. In 1838 Lenz demonstrated that current flow direction is responsible , removal of heat from junction for freezing water into ice, or by changing current direction, besides heat is generated for melting ice.Heat energy absorbed or generated at the junction is dependent on electrical current.Proportionality constant is named **Peltier coefficient**. When a current is made to flow through a circuit, heat is released at upper junction (at T_2), and absorbed at lower junction (at T_1).Peltier heat assimilated by lower junction per unit time is represented by **Q** and its value is calculated by formula given below[11].

$$\mathbf{Q} = \boldsymbol{\Pi}_{\mathbf{AB}}\mathbf{I} = (\boldsymbol{\Pi}_{\mathbf{B}} - \boldsymbol{\Pi}_{\mathbf{A}})\mathbf{I} \qquad (1.2)$$

Where ,Π_{AB} represent Peltier coefficient of thermocouple made of material A and B. Π_A and Π_B represents Peltier coefficient of material A and B.Peltier coefficient value depends upon material temperature variation.In case of p-type silicon peltier coefficient value is positive for temperature below ~ 550 K and its value is negative for n-type silicon.

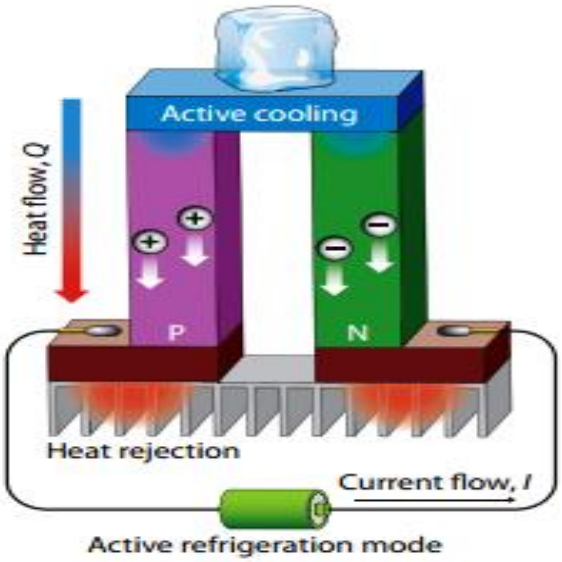

Figure 1.2 Peltier effect

The Peltier coefficients represent how much heat current carries in a unit charge, Since charge current must be continuous across a junction, the associated heat movement will create discontinuity if Π_A and Π_B are different. This leads to non-zero divergence at junction and thus heat need to be collected or consumed there, depending on sign of the current. For purpose of understanding Peltier effect based cooling of junction is to observe that when electrons flow according to its concentration gradient, this movement of electron results in cooling. The carriers will attempt to return to the electron concentration equilibrium that prevailed before the current was applied by absorbing energy at one connector and releasing it at second connector. This phenomena can be enhanced by series connection of individuals thermocouple. An important conclusion of this effect is that heat flow direction is related to polarity of current; changing polarity will result in direction change of heat transfer and thus changes sign of heat absorbed/evolved.

1.2.3 Thomson effect

In 1851 William Thomson ,released a detailed illustration of Seebeck and Peltier effects[12] and explained their association (called Kelvin Relations).Seebeck coefficients and Peltier coefficients are related through thermodynamics.Peltier coefficient is solely the multiplication of absolute temperature with Seebeck Coefficient. This thermodynamic inference enabled Thomson to forecast new thermoelectric effect, which was later called Thomson effect.

In Thomson effect heat may be assimilated or liberated when current made to flow in a material which have temperature difference. Heat is dependent on electrical current and temperature difference. Thomson coefficient is associated by thermodynamics with Seebeck coefficient.

If current density 'J' travel through uniform conductor, heat production in a unit volume is calculated by

$$\mathbf{q = \rho J^2 - \mu J \frac{dT}{dx}} \qquad (1.3)$$

Where, 'ρ' is the resistivity of the material

'dT/dx' is the temperature gradient along the wire

'μ' is the Thomson coefficient.

The first term 'ρJ²' is simply the Joule heating, which is not reversible.

The second term is the Thomson heat, which changes sign when J changes direction.

1.3 THERMOELECTRIC CHARACTERISTIC FEATURES

1.3.1 Power Factor

Seebeck coefficient is not at all the only parameter which conclude the utility of a material in thermoelectric generator or cooler.For given temperature difference, capability of material to generate useful electrical power is quantified by its power factor,

$$\textbf{Power factor} = \sigma S^2 \qquad (1.4)$$

Where, S is Seebeck Coefficient and σ is Electrical conductivity. Materials with large power factor are capable of producing higher energy in space confined application, but they are not certainly very efficient.

1.3.2 Device efficiency

The efficiency of thermoelectric materials device for electricity generation is given by η, defined as

$$\eta = \frac{\textbf{Energy provided to the load}}{\textbf{Heat energy absorbed at hot junction}} \qquad (1.5)$$

capability of given material to efficiently produce thermoelectric power is linked with dimensionless Figure of Merit(ZT) which is given by:

$$ZT = \frac{S^2 \sigma T}{\kappa} \qquad (1.1)$$

ZT value depend upon thermal conductivity (K), seebeck coefficient (S) and electrical conductivity (σ), and temperature (T).In thermoelectric devices, two materials are employed. η_{max} which is maximum efficiency is calculated by

$$\boldsymbol{\eta_{max} = \frac{T_H - T_C}{T_H} \frac{\sqrt{1+Z\bar{T}}-1}{\sqrt{1+Z\bar{T}}+\frac{T_C}{T_H}}} \quad (1.6)$$

Where, T_H is temperature of hot junction and T_C is temperature of cool surface. *ZT* is altered figure of merit, it is a dimensionless quantity which acknowledges thermoelectric capacity of thermoelectric materials used in designing of device and, after geometrical optimization [13], is defined as

$$\boldsymbol{Z\bar{T} = \frac{(S_p - S_n)^2 \bar{T}}{[(\rho_n \kappa_n)^{1/2} + (\rho_p \kappa_p)^{1/2}]^2}} \quad (1.7)$$

where,ρ is resistivity, T is mean temperature between hot and cold surfaces , subscripts n and p represents n and p type of semiconducting thermoelectric materials. Thermoelectric materials based devices efficiency is restricted by Carnot efficiency, due to which T_H and T_C terms are present in η_{max}.The coefficient of performance of present industrial thermoelectric refrigerators varies from 0.3 to 0.6, which is 0.166 times the value of conventional vapor-compression refrigerators [14].

1.3.3 Phonon-glass, electron-crystal behavior

Thermoelectric efficiency equations shown above thermal and electrical conductivity compete with each other. G. A. Slack proposed that in order to optimize the figure of merit, phonons, which are responsible for thermal conductivity must experience the material as they would in a glass (experiencing a high degree of phonon scattering-lowering thermal conductivity) while electrons must experience it as a crystal, (experiencing very little scattering-maintaining electrical conductivity). The figure of merit can be improved through the independent adjustment of these properties.

1.3.4 Effect of Semiconductor Behaviors

Semiconductors are ideal thermoelectric devices because of their band structure and electronic properties at high temperatures. Device efficiency is proportional to *ZT*, so ideal materials have a large Z value at high temperatures. Since temperature is easily adjustable, electrical conductivity is crucial.Particularly,reducing electrical conductivity at high temperatures and minimizing thermal conductivity optimizes ZT.

1.3.5 Thermal conductivity

$$\kappa = \kappa_{electron} + \kappa_{phonon} \qquad (1.8)$$

According to the Wiedemann -Franz law, higher the electrical conductivity, then higher the value of $\kappa_{electron}$ become [15].For that reason it is essential to reduce $\kappa_{phonon.}$ In semiconductors, $\kappa_{electron} < \kappa_{phonon}$, so it is favourable to disengage κ and σ in a semiconductor by engineering $\kappa_{phonon.}$

1.3.6 Electrical conductivity

Metals are good electrical conductors, but at higher temperature their conductivity reduces. This phenomena can be explained (approximately) in terms of the Drude conductivity formula:

$$\sigma = ne^2\tau/m \qquad (1.9)$$

'n' is charge carrier density

'e' is charge per carrier (elementary charge)

'τ' is carrier mean free time between scattering events

'm' is carrier mass

As temperature increases, τ decreases while the other numbers stay constant, thereby decreasing σ_{metal}.

In comparison, the electrical conductivity of semiconductors normally increases with temperature. In semiconductors, carrier mean free time decreases with increasing temperature, however carrier density increases faster with increasing temperature, resulting in increasing $\sigma_{semiconductors}$ [16].

1.3.7 State density

The band structure of semiconductors offers superior thermoelectric effects than that of metals. The Fermi energy is below the conduction band causing the state density to be asymmetric around the Fermi energy. Therefore, the average electron energy of the conduction band is higher than the Fermi energy, making the system conductive for charge motion into lower energy state. By contrast, Fermi energy lies in the conduction band in case of metals. This makes state density symmetric about Fermi energy so that average conduction electron energy is near to Fermi energy, reducing forces and pushing for charge transport. Therefore, semiconductors are ideal thermoelectric materials[17]

1.4 FIGURE OF MERIT (*ZT*)

In 1949 Abram Fedorovich loffe developed the modern theory of thermoelectric using the concept of "figure of merit" ZT, culminating in the classic texts on Semiconductor Thermoelements and Thermoelectric Cooling [18]. Materials with high thermoelectric figure of merit are typically heavily doped semiconductors, the best known are the tellurides of antimony, bismuth and lead. Efficiency of the thermoelectric material is measured in terms of a physical quantity known as figure of merit.It is given by:

$$\boldsymbol{ZT = \frac{S^2 \sigma T}{\kappa}} \qquad (1.1)$$

Where ZT = figure of merit, S = Seebeck's coefficient,σ = electrical conductivity, T=Temperature and K= thermal conductivity.

In the investigation of high ZT materials, a general strategy guided by the quality factor has been to look for small band gap semiconductors made from heavy elements. It is one

of the important parameters which decide that what material has good thermoelectric efficiency. A lot of research work throughout the world is being carried out to synthesize the materials which can result high figure of merit. The value of figure of merit near 1 to 2 is required to put thermoelectric material in industrial use [19]. But attaining this value is still a difficult task. In this work efforts have been made to synthesize the thermoelectric material which may improve the value of figure of merit.

1.5 APPLICATIONS AND USES

1.5.1 Power generation

Almost 90% of the electricity is generated by heat energy in today's world ,general efficiency of these system is 30–40% due to which approximately 15 terawatts of power is lost to the environment in the form of heat. By Thermoelectric devices we can transform this waste heat into useful electricity [20]. Thermoelectric efficiency depends on the ***figure of merit***, ZT. There is no theoretical upper limit to ZT, and as ZT approaches infinity, the thermoelectric efficiency approaches the Carnot limit. Thermoelectric generators serve application niches where efficiency and cost are less important than reliability, light weight, and small size.

Internal combustion engines capture 20–25% of the energy released during fuel combustion [21]. Increasing the conversion rate can increase mileage and provide more electricity for onboard controls and creature comforts (stability controls, telematics, navigation systems, electronic braking, etc). It may be possible to shift energy draw from the engine (in certain cases) to the electrical load in the car, e.g. electrical power steering or electrical coolant pump operation [22].

Cogeneration power plants use the heat produced during electricity generation for alternative purposes. Thermoelectric may find applications in such systems or in solar thermal energy generation [23].

1.5.2 Refrigeration

Thermoelectric materials can be used as refrigerators, called "thermoelectric coolers", or "Peltier coolers" after the Peltier effect that controls their operation. As a refrigeration technology, Peltier cooling is far less common than vapor compression refrigeration. The main advantages of a Peltier cooler (compared to a vapor-compression refrigerator) are its lack of moving parts or circulating fluid, and its small size and flexible shape (form factor). Another advantage is that Peltier coolers do not require refrigerant fluids, such as chlorofluorocarbons (CFCs) and related chemicals, which can have harmful environmental effects [24].

The main disadvantage of Peltier coolers is that they cannot simultaneously have low cost and high power efficiency. Advances in thermoelectric materials may allow the creation of Peltier coolers that are both cheap and efficient. It is estimated that materials with ZT>3 (about 20–30% Carnot efficiency) are required to replace traditional coolers in most applications [25]. Today, Peltier coolers are only used in niche applications.

1.5.3 Temperature measurement

Temperature difference between two objects can be measured by Thermocouples and thermopiles which is an application of Seebeck effect .Temperature difference measurement between two objects is done by connecting one object to the probe and other to a voltmeter.The temperature of the voltmeter and the material can be measured by the probe,it can also be measured separately by using cold junction compensation techniques.

1.5.4 Thermal cyclers for polymerase chain reaction

Thermal cyclers are laboratory devices which is based on Peltier effect.Thermal cyclers are mainly used for amplification of DNA by polymerase chain reaction(PCR).Periodic heating and cooling of samples at certain temperature is required for PCR.Incorporation of large quantity of thermocouples in a small space enables many samples to be amplified in parallel.

CHAPTER 2

LITERATURE REVIEW

2.1 Bismuth Telluride – Thermoelectric Material

Bismuth Telluride is an efficient thermoelectric material for room temperature applications and its alloy are also very efficient in same temperature range. Proposed application of Bismuth telluride are energy transformation, thermal sensors and thermoelectric cooler etc.

Bismuth telluride (Bi_2Te_3) is a semiconductor material. Its thermoelectric proficiency ameliorated by blending it with antimony or selenium which has plausible applications such as power generation or refrigeration. Bi_2Te_3 exhibits various density – reliant physical properties since it is a topological insulator. It is grey colour in appearance.

There are various different material systems undergoing research that have promising thermoelectric properties. Probable TE material systems were recently investigated by Kanatzdis [24], and figure 2.1 shows proposed thermoelectric materials with figure of merit (ZT) value with respect to temperature.

Bismuth telluride based compounds are remarkable thermoelectric materials at 300K [25-28]. However, the ZT of the bulk Bi_2Te_3 based materials has not improved obviously and has been approximately 1 for many years[24,29]. Efforts are made to improve the thermoelectric properties of bismuth telluride which are related to processing, composition and doping with other heavy metals[30-34].Current research focus on cutting down lattice thermal conductivity and enlarging electrical conductivity that exhibit large power factors [35]

Thermoelectric materials are categorized in different categories based on the temperature range of operation. Materials synthesized using bismuth telluride have highest ZT near room temperature but can not be operated above 523K. Lead telluride has second largest mean value of ZT in operating temperature range of up to around 773K. Ultimately, silicon and germanium has the lowest ZT and works for bigger duration at temperature around 1273K [25,29,36].

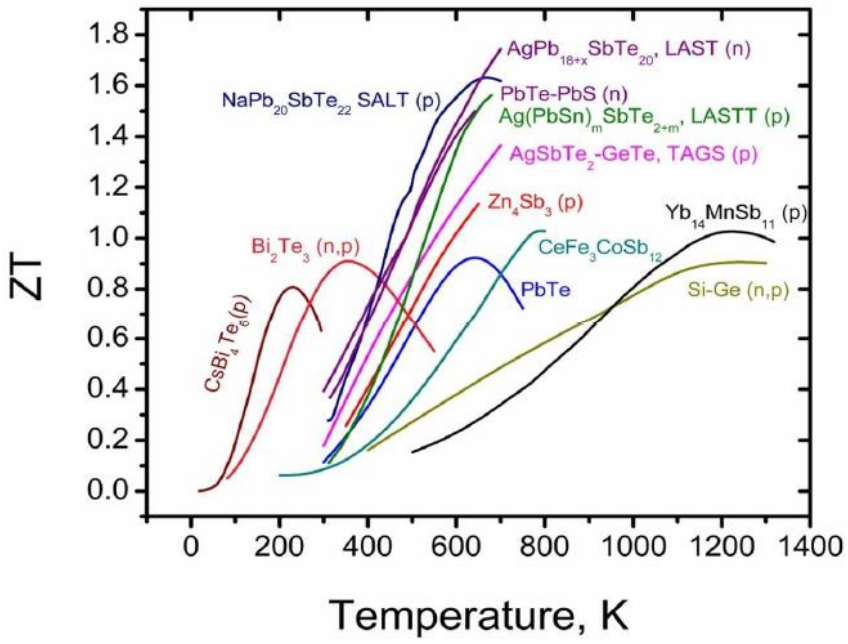

Figure 2.1 Showing the ZT values with respect to temperature for various thermoelectric materials studied. (Courtesy : M. G. Kanatzidis, Chem. Mater. ,22,648(2010)).

2.2 Structure of Bismuth Telluride

Bismuth telluride (Bi_2Te_3) and its compound are substantially exploited thermoelectric materials. It is a layered structure semiconductor which has topologically protected surface states and have narrow band gap (0.15eV)[37,38]. Bi_2Te_3 is a wonderful thermoelectric materials for thermodynamic cooling , thermodynamic heating and power generation[39-41]. The crystallographic structure of bismuth telluride is analogous with bismuth selenide and antimony telluride. Unit cell of bismuth telluride is rhombohedral. It comprises of five atoms per cell (two Bi, three Te).It is handy to examine structure Bi_2Te_3 by a hexagonal primitive cell. Hexagonal cell of bismuth telluride contains a set of layers perpendicular to c-axis. Plane hexagonal lattice is established by equivalent atoms of isolated layers. Array of atomic layers $Te^{(1)}$-Bi-$Te^{(2)}$-Bi-$Te^{(1)}$ [Figure2.2] exist in lattice. Above grouping of atoms is labeled as octet and triple octet mold hexagonal cell. Bi_2Te_3 carves easily along the planes perpendicular to c axis because of weak inter atomic bonding among adjacent tellurium atoms [42]. Bi_2Te_3 characteristics are mostly direction dependent due to existence of layered structure. Because of weak interatomic attraction

$Te^{(1)}$-$Te^{(2)}$ chain exist [43,44] while Te(1) – Bi and Bi-Te(2) are of ionic –covalent type[45,46]

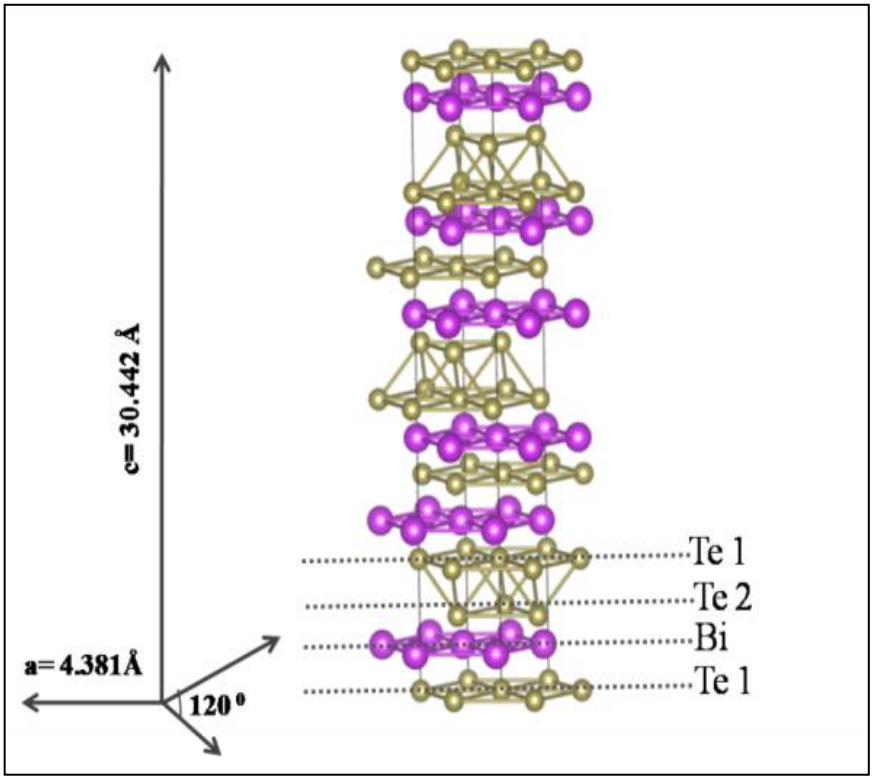

Figure 2.2 Layered structure of a Bi_2Te_3 crystal in hexagonal system.

Isomorphic solid solutions can be cultivated from compounds of Bi_2Te_3, Bi_2Se_3 and Sb_2Te_3. Since identical crystal arrangement is possessed , identical chemical features and lattice parameters. Covalent semi-diameter for Se, Bi, Te and Sb corresponds to 1.16,1.46,1.36 and 1.40Å, respectively.

2.3 Properties as Thermoelectric Materials

Bismuth telluride is a tiny band gap semiconductor material superimposed with trigonal unit cell. Conduction band and valence band arrangement comprises of reflection plane centered six standardized-energy ellipsoids [47]. Bi_2Te_3 carves easily along the planes perpendicular to c axis because of weak inter atomic bonding among adjacent tellurium atoms. Polycrystalline composed bismuth telluride compound material favourable for

cooling, heating and energy formation .At 300K, Seebeck coefficient of bulk Bi_2Te_3 reduces. Mix of bismuth, antimony, tellurium, and selenium must be employed for energy generation [48].

In recent past, researchers do their level best for raising performance of Bi_2Te_3 contained compound by constructing structures where one or more dimensions are scaled down, such as thin films or nanowires. In an attempt revised seebeck coefficient of n-type bismuth telluride is −287 μV/K at 327K [49]. There exist tradeoff between Electrical conductivity and Seebeck Coefficient , higher value of seebeck coefficient leads to lower value of electrical conductivity because of fall in carrier concentration[50].

In particularly different investigation researchers recorded higher value of electrical conductivity of Bismuth Telluride which is 1.1×10^5 S·m/m^2 and exceptionally small lattice thermal conductivity of 1.20 W/(m·K) [51].

Bismuth telluride and bismuth telluride composed alloys has applications such as commercial peltier elements since near room temperature figure of merit is excellent. Generally synthesized triple alloys comprises bismuth telluride with either bismuth selenide or antimony telluride [52].Their crystal structure is hexagonal [53], it is also reported by some researchers that unit cell is rhombohedral [54]. Hexagonal characterization outline laminated structure of material, and lattice constants of its unit cell are a = 4.38Å and c = 30.36Å [55]. Comparable linear thermal expansion coefficients are 14.4 $x10^{-6}K^{-1}$ and 21.3 x $10^{-6}K^{-1}$ [33,34]. Density of Bi_2Te_3 is 7.86g/cm^{-3} ,its wide temperature range thermoelectric applications is limited by its melting point of 858K [56].

At 300K , Bismuth telluride band gap energy is 0.15eV. It has modest value of band gap and an indirect band gap semiconductor material. Band gap of semiconductor material decreases with rise in temperature[57,58]. In accordance with quasi-potential band structure estimations [59,60], both valence band and conduction band have six valleys. Concentration of higher energy levels is comparatively high because of small density of states[51]. By first principle calculations research work concluded a short time ago

[62,63],first principle calculations work as fundamental principle for performance improvement by inclusion of low-dimensional structures [64].

It is possible to increase figure of merit by decreasing magnitude of thermal conductivity. Lattice thermal conductivity depends upon phonon scattering contributed by dopants [65]. In sintered samples by grain boundary scattering it is possible to curtail lattice thermal conductivity [66].

Table 2.1 Properties of Bismuth Telluride

Molecular formula	**Molar Mass (gm/mol)**	**Appearance**	**Density (gm/cm^3)**	**Melting Point(°C)**	**Crystal structure**
Bi_2Te_3	**800.761**	**Grey powder**	**7.7**	**585**	**Trigonal**

Electrical Conductivity(S/m)	**Thermal Conductivity (W/m/K)**	**Seebeck Coefficient(μV/K)**	**Figure of merit (ZT)**
1.1×10^5	**1.20**	**-287**	**0.953-1.012**

[Courtsey:(1) D.M.Rowe,University of Wales Cardiff,U.K.CRC Handbook of Thermoelectric
(2) H.J.Goldsmid,Introduction to Thermoelectricity,Springer-Verlag BerlinHeidelberg.]

2.4 Improving figure of merit (ZT)

Large scale industrial application of any thermoelectric material is dependent on the value of ZT i.e. figure of merit. TE material Bi_2Te_3 applications will depend on the value of ZT ,higher the value ZT better will be the efficiency and less wastage of energy. In present study main aim is to improve the value of ZT either by increasing the value of electrical conductivity or by reducing the value of thermal conductivity.

By the help of following methods it is possible improve the value of ZT.

- Increasing electrical conductivity.
- Reducing thermal conductivity
- Increasing thermoelectric power (Seebeck Coefficient)

Thermal conductivity of a material depends on electrons and phonons. It is more favourable to reduce phonon conductivity than the thermal conductivity which depends on electrons. Since the flow of electrons due to thermal potential contributes in thermoelectric emf. There will be decline in value of phonon conductivity of material by increment in number of interfaces encountered by phonons in material. The number of interfaces in materials can be increased by following methods:

- By inclusion of nanoparticles in bulk material, due to lower dimension of nanoparticles there will be large number of interfaces for phonon.
- By incorporating nano structured materials.

In this work CNTs(Carbon nanotube) are deployed for reinforcement in bismuth telluride composites for improving its thermoelectric efficiency. Here brief introduction of CNTs properties and its application is necessary.

2.5 Carbon Nanotubes (CNTs)

Carbon nanotubes (CNTs) are barrel shaped nanostructures which are allotropes of carbon. Nanotubes are manufactured with great length to diameter proportion of up to 132,000,000:1 [67], incomparably and significantly larger than any spare material. Unique characteristics are shown by cylindrical carbon molecules due to which it has wide application in field of materials science which includes nanotechnology and electronics. CNTs are also employed in the manufacturing of bulletproof vest. They have exclusive electrical properties and exceptional strength.

Nanotubes are member of fullerene structural family, which also contains buckyballs [68]. Boundary of nanotube is closed with hemisphere of buckyball structure. Name of carbon nanotube is acquired from their dimension, since diameter of a nanotube is few nanometers(approximately $1/50{,}000^{th}$ of width of a human hair), while they can be up to 18 centimeters in length [69]. Nanotubes are categorized as single-walled nanotubes (SWNTs) and multi-walled nanotubes (MWNTs).

2.5.1 Types of Carbon Nanotubes

CNTs are graphene sheets rolled in the cylindrical form. As result of there cylindrical structure they have two dimensional confinement of electrons. During the formation of CNT graphene sheet can be folded in different forms giving rise to various types of carbon nanotubes.

Depending upon the number of concentric cylinder CNTs can be [70]:

- Single walled Carbon nanotubes (SWCNT): having single wall of graphene cylinder.
- Multi-walled carbon nanotubes (MWCNT): having 2 or more concentric walls of graphene cylinder.

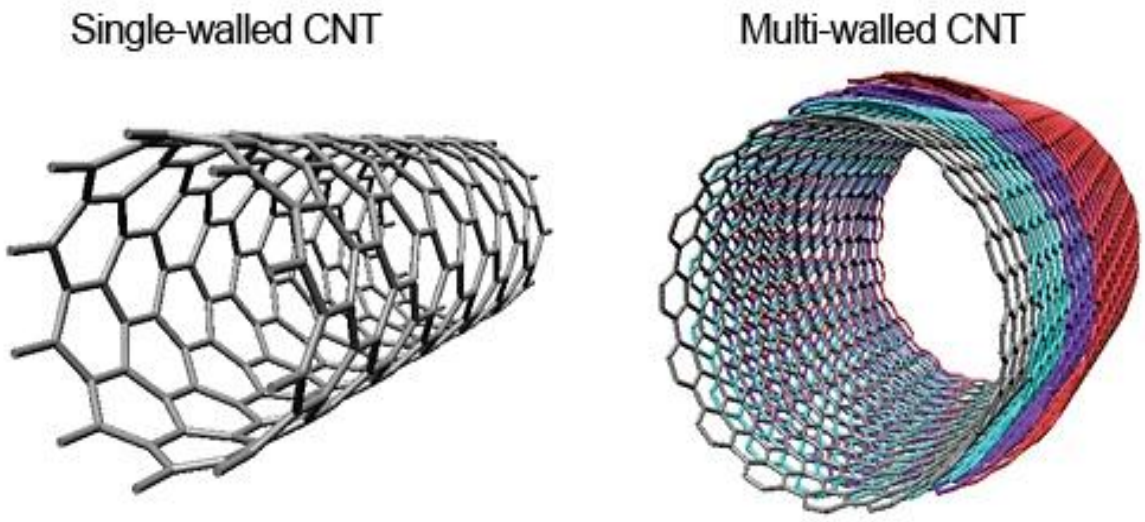

Figure 2.3 Single-walled and multi-walled CNTs

Properties of SWCNTs is superior with respect to MWCNTs but synthesis of MWCNTs is much easier. In research field MWCNTs are more popular. In this research MWCNTs were used as reinforced material to make Bi_2Te_3 nanocomposite. SWCNTs are further of three types depending upon how graphene sheet is folded.

- Armchair
- Zigzag
- Chiral

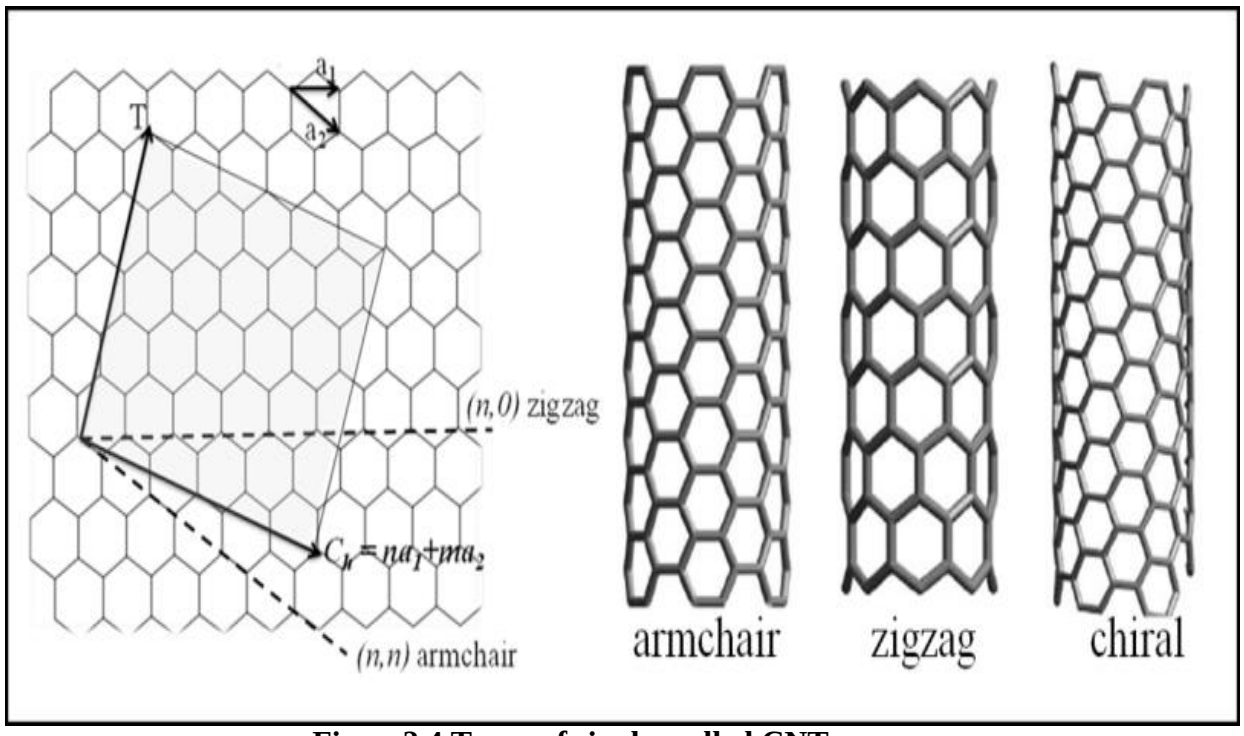

Figure2.4 Types of single-walled CNTs

Table 2.2 Properties of CNTs.

Mechanical	Electrical	Thermal	Chemical
• Strong and flexible • Young's modulus:1Tpa • High aspect ratio	• Electrical conductivity 6 times of copper • Can metallic or semi-conducting depending on chirality • High current density	• Thermal conductivity of single CNT is very high of the order of 2000W/m/K • CNT in bulk have thermal conductivity of just 20-200W/m/K [71]	• CNTs can easily be functionalized making them quite useful carrier

(Courtsey:Single wall Carbon nanotubes:two ways of production,Syn.Met103,2488(1999))

2.6 Reason for using Carbon nanotubes

Since CNTs has spectacular properties they are preferable material for improving the thermoelectric efficiency of Bismuth Telluride nanocomposites.

- Surface to volume ratio of CNT is very high, aspect ratio is also very high. So phonon scattering will be high because of high surface area in bulk [72].

- CNTs has very high value of electrical and thermal conductivity. Reinforcement of CNTs improves electrical conductivity of the material. Random arrangement of CNTs in bulk results in low amount of thermal conductivity around 20-200W/m/K[73]. There will be decrease in value of phonon thermal conductivity if CNTs are added in bulk .

CNTs reinforcement in Bismuth Telluride will result in improvement of thermoelectric efficiency. Generation of ingot of bulk Bismuth Telluride by directional solidification method and formation of CNTs reinforced Bismuth Telluride nanocomposites are discussed in next chapter.

CHAPTER 3

SYNTHESIS

In this chapter detailed discussion about generation of ingot of bulk Bismuth Telluride and synthesis of MWCNTs reinforced bismuth Telluride composites. Bulk ingot was synthesized by vertical directional solidification technique.

3.1 Phase Diagram

For synthesis of formidable quality Bismuth Telluride compound with stoichiometric composition, detailed understanding of Bi-Te phase diagram is must. Figure3.1 represents the phase diagram of Bi-Te compound[74]. At 586°C the solidus phase of Bi_2Te_3 was obtained and below this temperature other phases of bismuth telluride were obtained. The wide miscibility range of Bi_2Te_3 has been split into two phases: Bi_2Te_3 with a narrow miscibility range and BiTe which forms peritectically at 540°C. The Bi_2Te has a large range of miscibility and forms by peritectic crystallization at 420°C

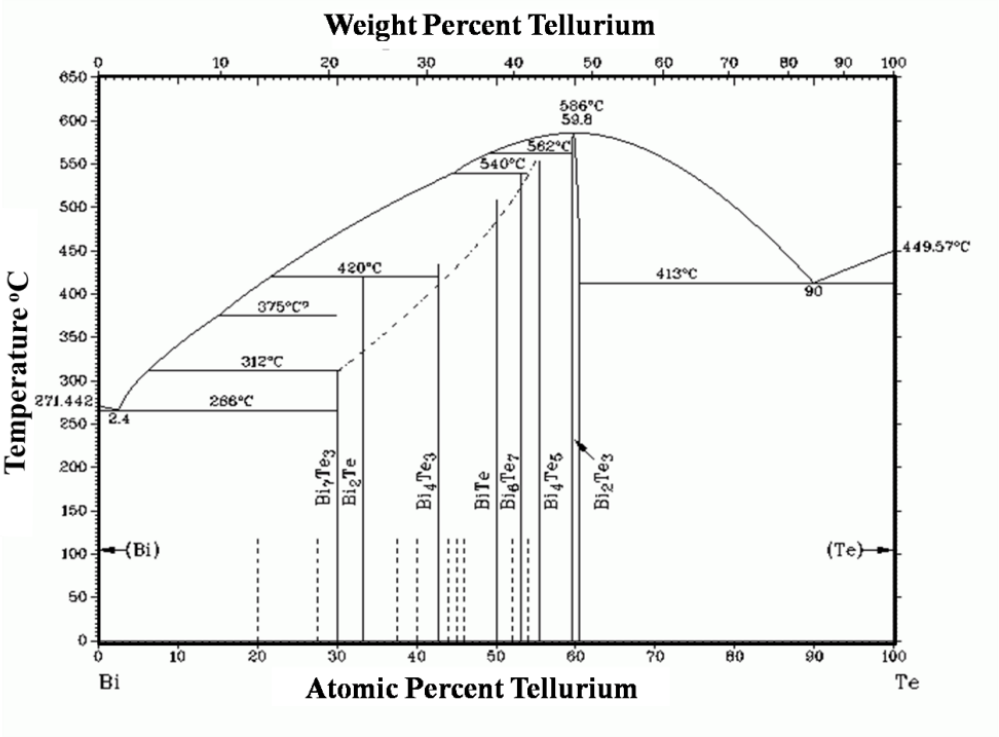

(Courtesy:B. Predel, Landolt-Bornstein-Group IV Physical Chemistry.,5b,1(1992)).

Figure 3.1 Phase Diagram of Bi_2Te_3

3.2 Directional Solidification

In directional solidification process molten metal is consolidated by well regulated method for the aim of constant availability of the consolidating front of casting with feed metal[74]. Bridgman growth of metal crystal takes place during the directional solidification. The Bridgman technique is a process of growing single crystal compounds. This method requires heating of polycrystalline material in a container at a temperature higher than its melting point and gently cooling it from one side where a seed crystal is placed[75]. By length of container single crystal material is grown gradually. It is possible to complete above process either in vertical setup or horizontal setup. Figure 3.2 depicts setup of vertical directional solidification process. Quartz ampoule is initially scorched to temperature higher than melting point of the metal and is kept at that temperature for the certain time period. Then ampoule will be lowered to cool zone which contribute towards the solidification and generation of single crystal along the downward direction [76,77].

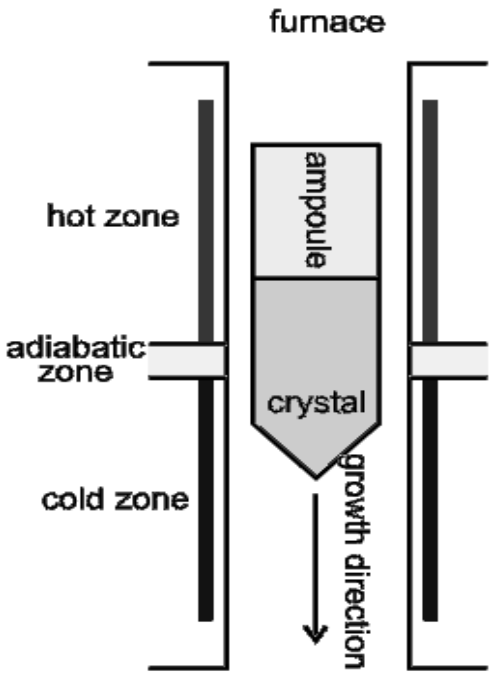

Figure 3.2 Vertical directional solidification

3.3 Synthesis of Bismuth Telluride compound

Bismuth Telluride (Bi_2Te_3) compound was grown by directional solidification technique using high purity (99.999%) elements. High grade Bi and Te were taken in stoichiometric proportion in a quartz ampoule .The sealed quartz ampoule was loaded in a vertical muffle furnace and heated to 750°C where it was kept for 3 hours in constant temperature zone for melting [78]. Then the ampoule was lowered to cool at a very small rate of 1cm/30min. The picture of the grown sample is shown below.

Figure 3.3 VDS grown Bismuth telluride Ingot.

Figure 3.4 High Temperature Furnace (Vertical Muffle Furnace).

Figure3.5 Quartz ampoule.

Figure 3.5 above shows the quartz ampoule used in the bulk growth of bismuth telluride compound.

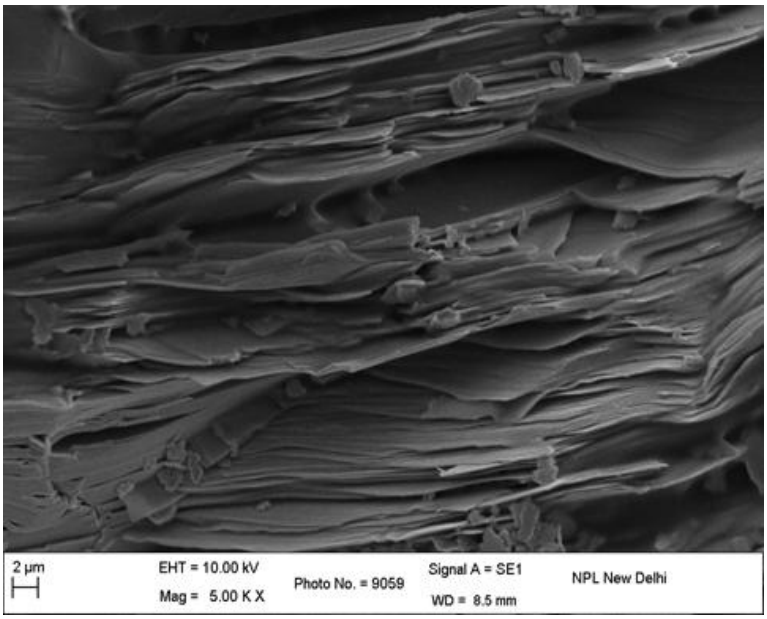

Figure 3.6 SEM micrograph of layered structure.

SEM micrograph shows the layered structure of the materials which break along its cleavages planes and corresponding EDS spectra confirms the stoichiometry .

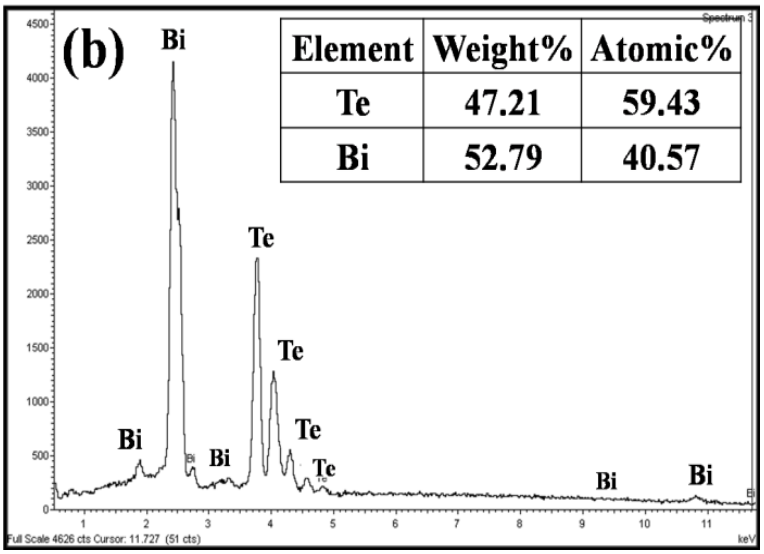

Figure 3.7 Shows the EDS spectra of bulk sample grown

3.4 Ball Milling (BM) Method

Ball mill is a type of grinder employed for grinding materials into extremely fine powder [79]. It is one of easiest and popular way of synthesizing nanoparticles of metals and composites in powder form. Genarally single or more than one containers are employed for ball milling large amount of samples. Very hard steel balls, tungsten carbide balls are placed in ball mill jar along with powder or flakes of sample under investigation. Ball to particle ratio is selected according to requirement of dimension reduction. If container is more than half filled then the efficiency of milling is reduced. Ball milling jar must be filled with inert gases like nitrogen or argon. A rise of temperature in the range of 100 to 1100°C takes place during milling process. Containers are rotated at high speed around their own axis. Although they can be rotated around some central axis and are therefore called as planetary ball mill. By monitoring speed of rotation of the central axis and container as well as duration of ball milling it is possible to grind the material to fine powder.

High-quality ball mills are very costly but can grind particles to as small as 5nm [80]. Basis of grinding is the value of critical speed. Speed after which steel balls starts circular

rotation along the axis of cylindrical device and further grinding is stopped is called as Critical speed [81].

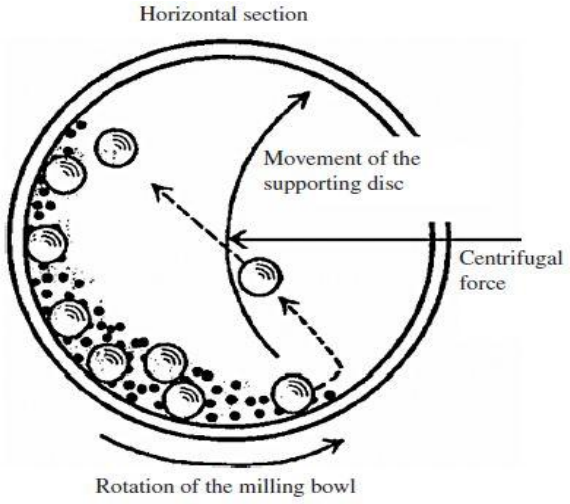

Figure 3.8 Ball Milling Process

3.5 Pellets formation by Spark Plasma Sintering

Spark plasma sintering (SPS) is a fast powder consolidation sintering technique which takes only a few minutes to complete a sintering process [82,83]. SPS is favourable for fabrication of thermoelectric materials because this technique is able to reduce grain growth which takes place during sintering [84,85,86]. In SPS , powder material was kept in graphite die and placed inside high vacuum chamber. A pulsed DC current passed through the die, this pulsed DC current momentarily generates plasma spark in the gap between the material particles. This spark discharge generates high temperature state of up to many thousands °C for a short period of time, in minute local areas between the particles. In the presence of pressure and electric currents, surface layers melt and fuse with each other and creating necks between particles. This short duration heating and vaporization of particles surfaces occurs faster due to joule heating during the SPS process. Consequently the temperature rises very fast and densification completed with in few minutes.

SPS is competent for powder material operation , however curiosity is generally large for nanocrystalline structures. Thermoelectric materials may well find improved

characteristics after using SPS. Thermal conductivity can be controlled by controlling grain growth. Controlling compression and temperature , Density of material, porosity is regulated very well by SPS technology while retaining strong particles bond in sample. Therefore, in thermoelectric materials thermal conductivity may be controlled by controlling the grain growth during SPS. By process of sintering already present contaminants and oxidizing agents gets vaporized. SPS results in stronger bond between particles. For composite materials ,high homogeneity is possible with either lower or higher density. Normal sintering techniques are cheaper than SPS and SPS is about 20 times faster.

Nanomaterials from Bi_2Te_3 bulk compound was prepared by using ball milling .Further SPS process was used to make pellets from ball milled nano powders. These pellets were used for further characterization. Figure below shows Spark Plasma Sintering setup at NPL.

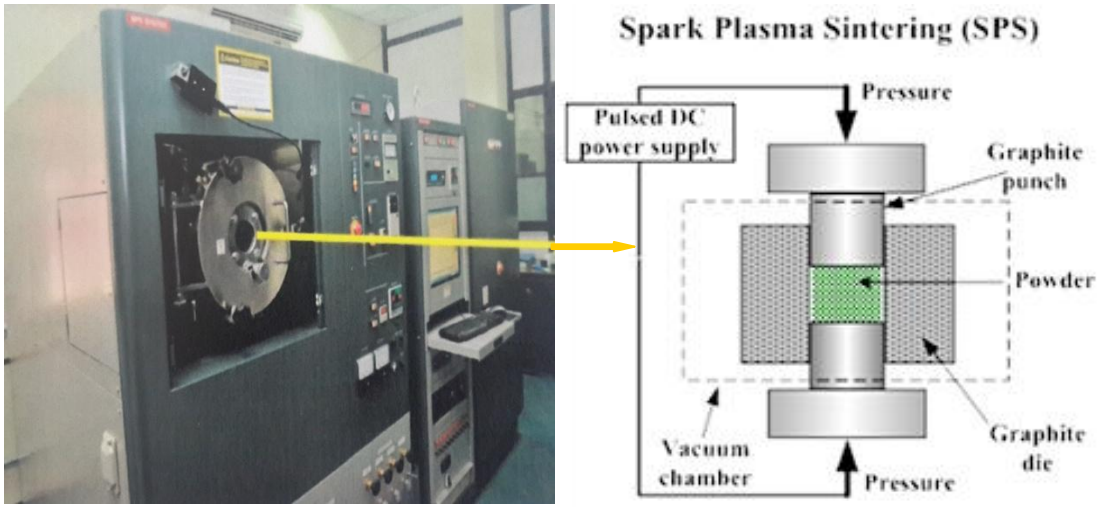

Figure 3.9 Spark Plasma Sintering.

3.6 Synthesis of Bismuth Telluride and MWCNTs nanocomposites

- By using mortar & pestle Bismuth Telluride ingot was grinded manually into powder .
- Inert atmosphere ball milling of Bismuth Telluride powder was performed for duration of 8 hrs.
- Then ball milled bismuth telluride powder was mixed with 1.5% & 3% by weight MWCNTs for preparation of two samples.
- Petroleum ether was then added in two samples and the sample was ultrasonicated for 90 minutes.
- Ultrasonication was done to resolve the entanglement of MWCNTs in the mixture.
- Two samples were further ball milled for 1 hour with 10:1 Ball Particle Ratio (BPR) in argon atmosphere.
- Two pellets were then made from from the two samples containing different percentage of MWCNTs.
- Spark Plasma Sintering technique was used for making Pellets .Since the thermal stability of the MWCNTs is very high i.e. around 3000K. So MWCNTs does not get damaged during the process of sintering.

CHAPTER 4

CHARACTERIZATION TECHNIQUES USED

In last chapter discussion about the synthesis techniques used in synthesis of Bismuth Telluride compound and nanocomposite. In this chapter discussion of various characterization techniques used to investigate them was done.

4.1 X-Ray diffraction (XRD)

The X-ray diffractometer machine used in this investigation was supplied by Bruker Model:D8 Advance , Bruker - AXS. It is an automatic powder X-ray diffractometer. X-ray diffraction is very popular and highly accurate investigating technique for phase identification of unknown synthesized materials. It is a radiation of electromagnetic waves having wavelength in the range of 0.1 to 100 Å.X-rays.

Principle of XRD

Basically X-ray powder diffraction technique involves a narrow beam of monochromatic x-rays impinging upon a crystalline powder composed of fine, randomly oriented particles. The crystallites which may be suitably oriented to satisfy Bragg's Law would give rise to diffracted rays in certain diffraction angles corresponding to particular sets of 'd' values and the wavelength of x-ray used. The diffracted rays may be recorded by camera technique using photographic film or diffractometer technique using a suitable detector along with electronic equipment for enhancing the detection limit and noise elimination.

In XRD operation monochromatic photon packet is allowed to fall at an angle θ upon specimen surface. The position of detector is set to fix with respect to the specimen for getting reflections at an angle θ. In order to fix the position of detector with respect to specimen we fix direction of incident beam and rotate specimen and detector or another way is by placing specimen fixed and rotating detector and incident beam in opposite directions. The crystallites which have reflecting planes (hkl) parallel or nearly parallel with respect to specimen surface enrich reflection intensities. Goniometer comprises of sample holder, detector arm and associated gearing in which tilts or rotation are carried out automatically. Figure4.1 shows the schematic diagram and photo of the XRD, respectively. The concentration of the phase , in quantitative analysis , is estimated by

evaluation of peak intensities and peak areas with correction made for non random orientation of the crystallites as well as diffraction line overlap.

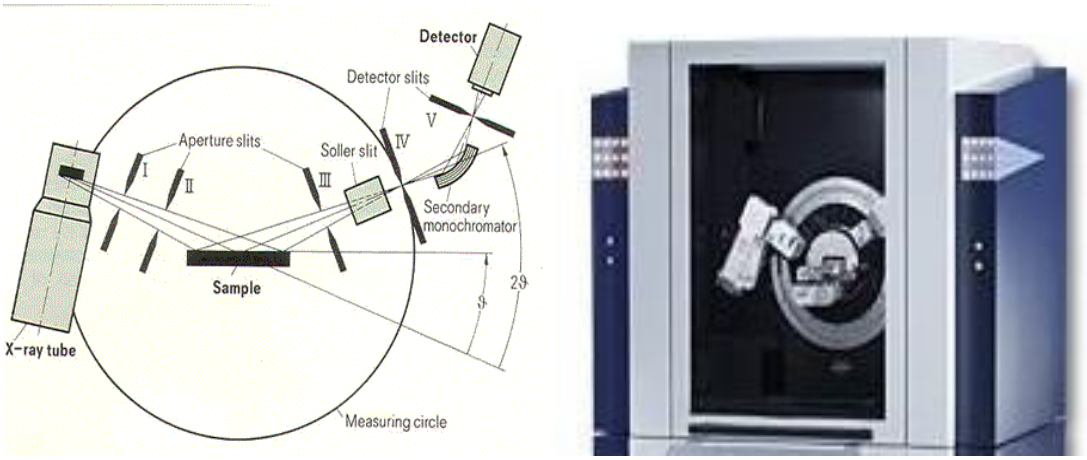

Figure 4.1 Schematic diagram and picture of XRD setup at NPL.

When beam of X-ray hits an electron of an atom in the crystal it generates secondary spherical waves in almost all directions, existing electrons of crystal are responsible for secondary spherical waves. By the phenomena of destructive interference the scattered waves cancel out one another in almost all possible directions. Atoms inside crystal are arranged in regular pattern ,and in some directions we have constructive interference calculated by Bragg's Law.

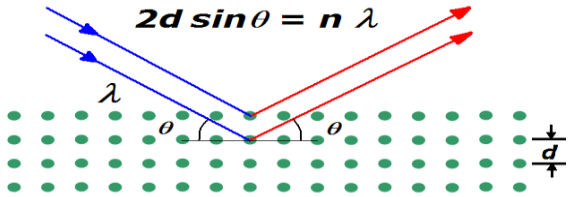

Figure 4.2 Bragg Reflections.

L.H. Bragg and W.H. Bragg experimentally proved that diffraction can be treated geometrically like reflection (Figure 4.2). They geometrically derived Bragg's Law, which represent diffraction in simple equations [87].

$$2d\,Sin\theta = n\lambda \qquad (4.1)$$

where, 'n' is order of reflection , 'λ' is wavelength of X-ray, 'd' is inter planar spacing and 'θ' is angle between lattice planes and incident beam.

X-ray diffraction technique is commonly used for identification of phases and crystalline structure of materials. Crystallite size (t) determined by using Scherrer equation:

$$Crystallite\ size\ (t) = \frac{K\lambda}{\beta Cos\theta} \qquad (4.2)$$

where, β is full width half maxima (FWHM), K is shape factor having value 0.94 and λ is the wavelength of X-ray used for diffraction.

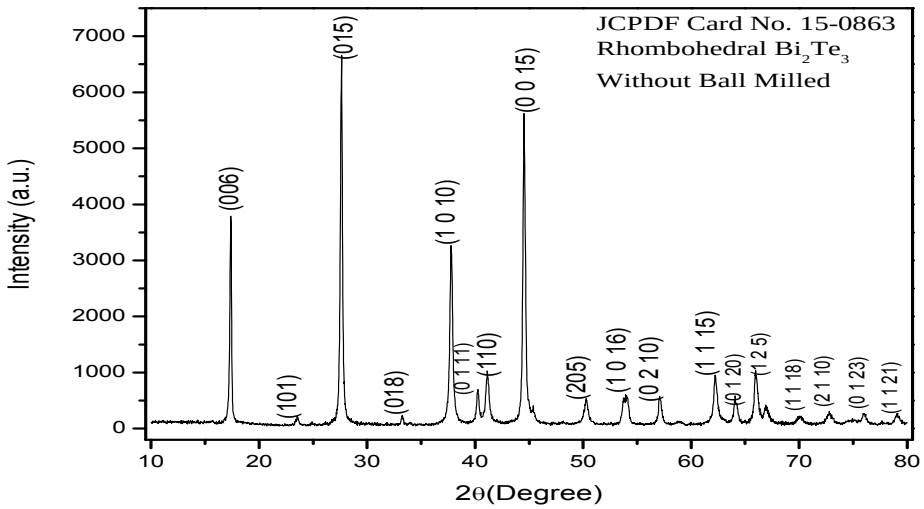

Figure 4.3: XRD spectrum of Bi_2Te_3

XRD is also used for investigation of imperfection in the crystals such as stress and strain [87,88].Force applied in unit area is known as stress. Residual stress stays in compound even after removal of external force. Positive values indicates expansion and negative values represent compression. Stress determination by XRD plot is related to distribution of lattice strain. The variation of unit length is known as strain. If d_o is the spacing between reflecting planes and by applying tensile strain it becomes d then respective diffraction line gets transferred towards smaller angles i.e. reflection at 2θ and from calculation of variation in d-spacing for different planes observed in sample.From differentiation of Bragg's Law it is possible to obtain equation relating broadening generated and non uniformity of strain.

$$b = \frac{-2\varepsilon}{Cot\theta} \qquad (4.3)$$

where, ε is elastic strain with the value, ε = $\frac{\Delta d}{d}$,and b is additional broadening , ratio of change in plane spacing Δd/d. Stress is calculated by multiplying mean strain Δd/d by elastic constant.

4.2 Scanning Electron Microscopy(SEM)

Semiconducting materials prepared by various techniques in different temperature conditions, shows different surface morphology when examined by scanning electron microscope. Surface morphology of the material assist in study of grain growth ,orientation of the grains, compositional and topographical features present on the surface of the material. From the surface structure it is possible to determine the compactness of the material, the particle size and shape, to compute the percentage area occupied by particular phase.

The scanning electron microscope (SEM) is an excellent tool for imaging and analysis of microstructure morphology and chemical composition characterizations. In the present work a high performance scanning electron microscope (SEM) model: EVO MA 10 with INCA 250 Energy EDS shown in figure 4.6 has been used to study morphological features of compound. It is a software controlled scanning electron microscope.SEM uses an electron beam for scanning surface of specimen. Electron beam generated by electron gun made of tungsten filament, LaB_6 filament, or FEGs. Because of good quality resolution and brightness FEG sources are employed for imaging , at lower voltages and has comparatively long life. Three lenses under the gun, shape and focus electron beam before it strike specimen in scanned or raster mode.

A turbo molecular pump , backed by a rotator pump ,is used to evacuate the specimen chamber. Normal operating vacuum in the chamber is of the order of 10^{-4} to 10^{-6} torr. In this work SEM was operated at 20 kV in the secondary electron image mode. In the case of conducting samples the surface morphology and surface structure were examined directly. However in the case of non-conducting samples, sample surface laminated by very thin layer (~10nm) of gold before examining with SEM in order to avoid charging effect and to improve the contrast.

Principle of SEM:

When packet of electrons hits the surface of specimen, a large number of signals are emitted from the specimen as a result of electron-matter interaction as shown in the figure 4.4. Electron beam strikes on the specimen leads to generation of secondary electrons , back scattered electrons, auger electrons and characteristic X-rays. These electrons can be detected by suitable detectors and provides knowledge about specimen micro structure and surface morphology.

Secondary electrons and backscattered electrons are utilized for generation of image of sample. Secondary electrons contributes in imaging of morphology and topography of specimen and backscattered electrons contributes in contrast of multiphase specimen.

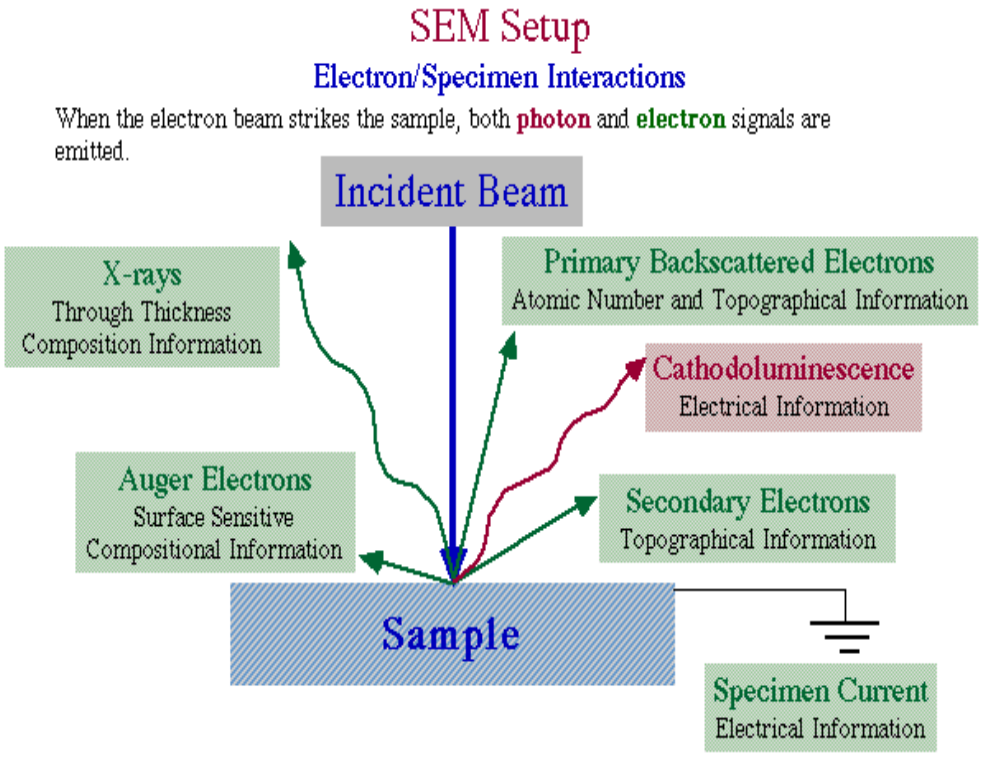

Figure 4.4 Schematic Diagram of electron-sample interaction.

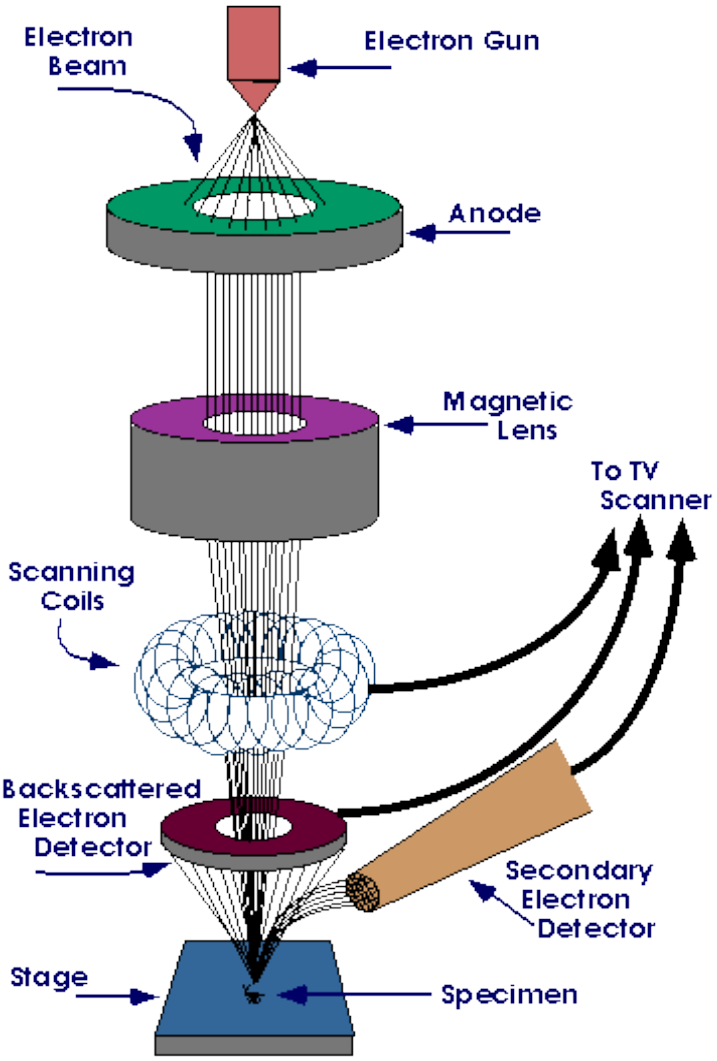

Figure 4.5 Ray diagram of SEM working.

4.2.1 Resolution and magnification of SEM

The instrument has a resolution 3.0nm SEI mode and 5.0nm BEI mode at variable working distances. The magnification on the computer screen can be varied from 5x to 300000x. Spatial resolution depends up the size of electron spot and the interaction volume. Spot size and interaction volume are very bigger in comparison with distance between atoms. Hence resolution of SEM is not large enough to image down to atomic scale but in case of transmission electron microscopy (TEM) it is possible to image down to atomic scale. SEM has an edge over TEM which includes capacity of imaging bigger

cross-section of sample and capacity to image bulk material, and various imaging quality options are present for investigating composition and nature of specimen.

Figure 4.6 SEM with EDS Facility at NPL.

4.2.2 Energy Dispersive Spectrometer (EDS):Elemental Analysis

The study of surface morphology of semiconducting materials by SEM gives an idea of various phases present in it. It becomes important to investigate the composition or elements present in each and every type of morphology for the identification of various phases formed in the material. For this purpose electron probe microanalysis has been carried out on each and every different grain showing distinct morphology. In the present case energy dispersive X-ray spectrometer with INCA 250 Energy EDS an attachment to SEM has been used for the determination of elemental composition. With EDS system used, it is possible to detect elements having atomic number 5 (Boron) to 92 (uranium).The resolution of the system is 133eV and accuracy of measurement is 0.5% wt qualitative, 0.1% wt quantitative.

Principle of EDS

X-rays originated from excited specimen hit the detector consisting of Si(Li) detector covered with thin beryllium window. These X-rays create electron hole pairs in the

semiconductor detector. Charge is dispensed to a field effect transistor (FET) in a preamplifier that is positioned close to the detector to reduce noise. The pre-amplifier obtains voltage pulse from charge pulse which then by help of pulse processor is boosted and chiseled and then passed into energy to digital converter(EDC). It acquires this shaped and amplified pulse, find the peak voltage of the pulse and transform its amplitude into discrete numerical value which is dependent upon amplitude of pulse and on energy of incident X-ray. Voltage pulses are further coded into numerical values and are stored according to their amplitudes.

The counts that are gathered in memory exhibit calculated X-ray energy spectrum and spectrum is displayed as histogram of number of x-ray counts measured(Y-axis) as function of x-ray energy(X-axis). Energy spikes along the x-axis represents the elements which are present in specimen. Quantity of x-rays generated rely on the number of atoms in specimen. There exist a detection limit for this system due to which the elements having atomic number less than 5 can not be detected. Useful spectra for desired analysis can be obtained in few minutes.

Applications of EDS

- Compositional analysis.
- X-ray mapping.
- Identification of second phase in matrix.
- Elements distribution in materials.

4.3 Transmission Electron Microscopy (TEM)

Transmission electron microscope is a major microscopy techniques for imaging internal microstructure of excessive fine samples [89]. The fundamental TEM instrument is depicted in Figure 4.7.

Principle of TEM

In TEM, an electron beam , which is almost parallel, is scattered by a thin specimen. The specimen thickness normally varies between 50 to 200nm. In case of the crystalline materials this scattering takes from one or two Bragg diffracted beams travelling in small angles (1or 2 degree) with incident beam. This diffracted beam is focused to form an electron diffraction pattern in rear focal plane and forms the image of the object on the central plane of anterior lens ,which is magnified by intermediate lenses and projector lens.

The electron gun is commonly thermionic tungsten but FEGs are becoming common. For operation of TEM accelerating voltage employed is larger than that used in SEM and is generally 100–400 keV [90]. Benefit of using high voltage include high imaging resolution, higher penetration power because of lower electron wavelength and by virtue of which it is possible to investigate of condenser lenses demagnify probe to typically 1 mm in diameter, although it is possible to reduce by the help of condenser–objective nanoprobe. Dimension of specimen must be small i.e. less than few hundred nanometer and in the form of 3mm diameter circular grid. Sample is fixed between pole pieces of objective lens [91]. Selected area diffraction (SAD) enables selection of very small specimen cross section for electron diffraction. Small areas (few nanometres in diameter) is choosen employing a focused probe in comparison to large area.

TEM samples are ultra thin disc type, prepared by cutting, mechanical polishing or chemical dissolution and further electropolishing [92] (for conducting materials) and chemical polishing (for semiconductors and ceramics) [93]. Powders may be grounded and dispersed onto an amorphous support film or on a circular metal grid.

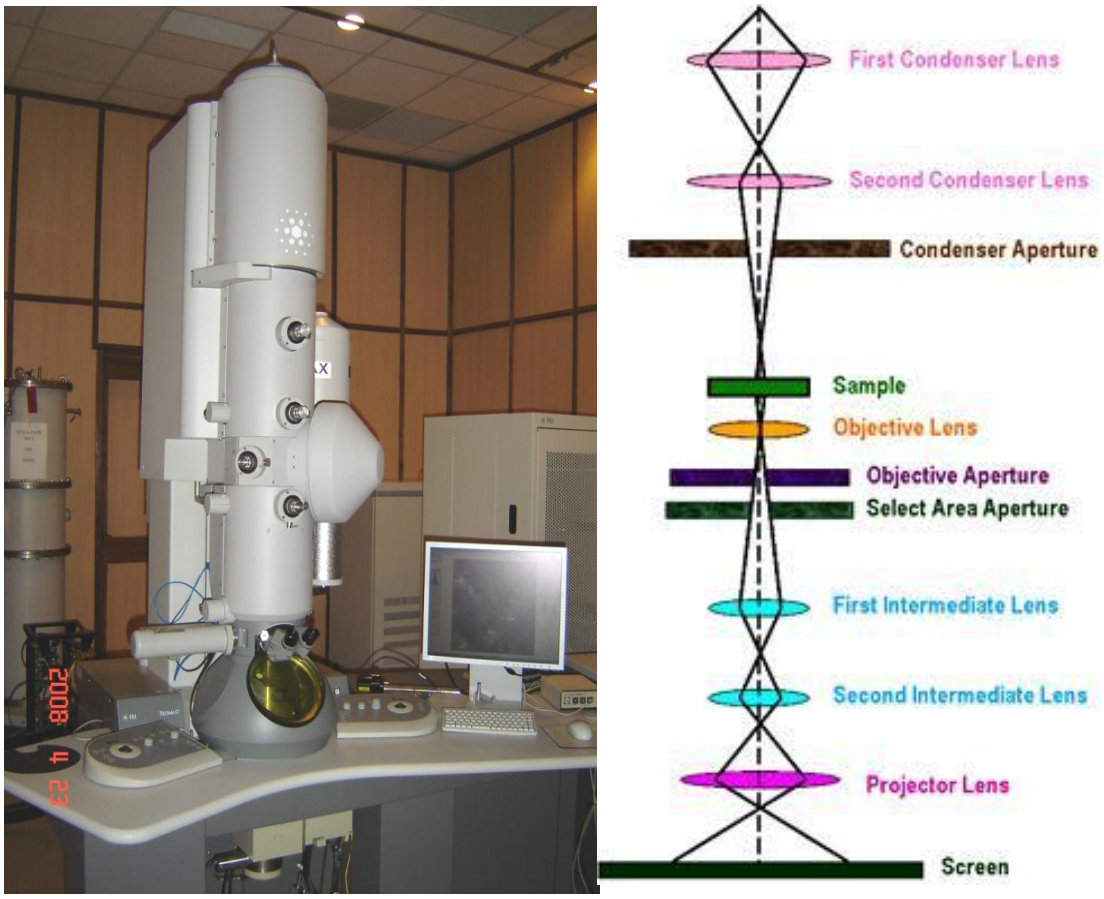

Figure 4.7 High Resolution Transmission electron microscope (HRTEM)

4.4 Electron Diffraction

Amorphous materials exhibits diffraction rings related to average interatomic distances. In crystalline materials, regular atomic arrangement deflects electrons by well-defined angles observed by Bragg's law (2.1). As value of λ is small (e.g., λ= 0.0037 nm for 100 keV electrons [94]), the Bragg angles are also small (of the order of 10^{-3} radians), sinθ ≈ θ and hence λ=2dθ [95]. Diffraction takes place only when planes of atoms are closely parallel to incident beam.

In case of a crystalline material, distinct spots are seen in electron diffraction pattern. In Figure 4.8 it was observed that area of specimen selected for diffraction pattern generation and identified by position of SAEDP aperture in TEM image. Patterns provides information about 3D crystal structure, symmetry of unit cell, sample quality and accurate lattice parameters upto an accuracy of 1 part in 10^4 [96].

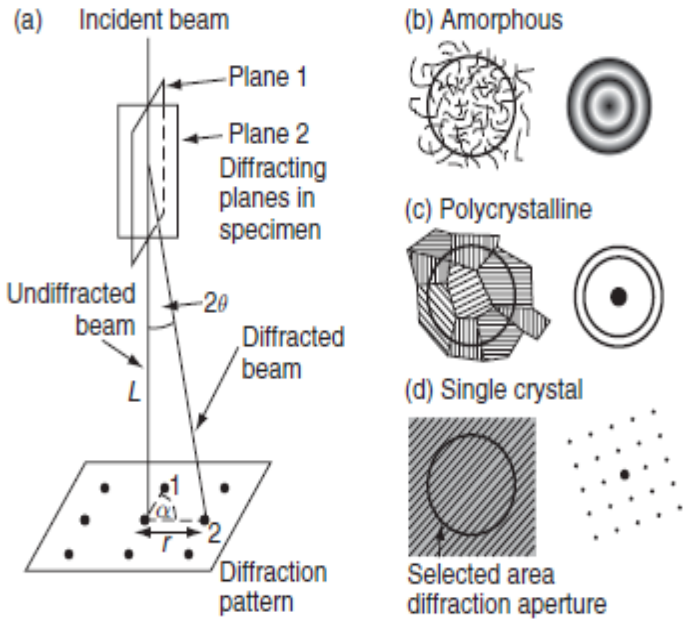

Figure 4.8 SAED patterns for different materials.

Bright and Dark Field images in TEM

When selected area electron diffraction (SAED) pattern is displayed on screen, diffraction pattern is suitable to execute two elementary imaging operations in the TEM. It is not related with type of specimen under investigating, the SAED pattern will contain a bright central spot which contains the direct electrons and some scattered electrons. Images in TEM can be obtained by using the central spot ,or by using some scattered electrons [97]. The choice of electrons to form the desired image can be made by embedding an aperture into posterior focal plane of objective lens, hence obstructing majority of electrons which are not needed to form a particular image. It is possible to use

the external drives to move aperture so that either direct electrons or some scattered electrons travel through it. If image formation is done by selecting direct beam then image generated is a bright field (BF) image [98].

A dark field (DF) image, as opposed to a bright field image is formed by obstructing transmitted electron beam and allowing the scattered electron beam of interest to pass through the aperture. The main advantage of dark field image observation is high contrast. Furthermore , the image resolution is comparable with that of the bright field image. The resultant lack of illumination brightness will necessitate an exposure time much longer than that for bright field image recording [99].

4.5 Hot Probe method (P-N type tester)

Carrier type measurement of the synthesized Bi_2Te_3 compound has been carried out by the hot probe method as shown in figure 4.9. This is simple, frequently used method, unencumbered by the necessity for the preparation of a special sample. One simply touches the unknown semiconductor surface by two identical metal probes, between which a galvanometer is connected.

One of the probes is heated while the other is at the room temperature. The hot probe immediately heats the semiconductor under it, with indirect hike in the kinetic energy of the free carriers there. Then these carriers moves with larger thermal velocities with respect to their cooler neighbors. Therefore these carriers diffuse out of the hot region faster than their slower neighbors can diffuse back into it from the vicinity. These results in the hot region becoming slightly depleted of majority carriers and acquiring the potential of the ionized impurities there, while the vicinity of the cold probe remains neutral. Current therefore will flow in the galvanometer, the direction of which depends on the ionized impurity. For N-type semiconductor, the hot probe is more positive one, while for P-type semiconductor it is more negative. The cold probe polarity therefore indicates the type. The experimental setup is shown in figure 4.10.

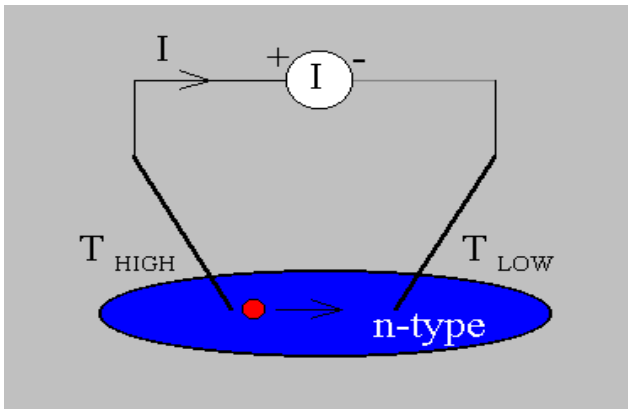

Figure 4.9 Sketch of Hot Probe

Figure 4.10 Experimental setup of P/N type tester.

Carrier type testing of VDS grown Bi_2Te_3 compound can be done by P/N type tester.VDS grown Bi_2Te_3 is n-type semiconductor compound.

4.6 Measurement of Thermal Conductivity

Measurement of thermal conductivity is a difficult task as thermal conductivity value depends on many factors like surface roughness, impurities, atmospheric temperature , humidity etc. Due to so many factors governing its value exact determination of thermal conductivity is difficult task. We will discuss the method that we have used for measurement –

4.6.1 Laser Flash Method

Thermal conductivity and diffusivity of solids, powders and liquids can be measured by laser flash method. In 1961, Parker, Butler, Jenkins and Abbott developed this method at U. S. Navy Radiological Defence Laboratory[100,101].

In this method , front surface of sample pellet is exposed to very small duration pulse of radiant thermal energy. Thermal energy of pulse is absorbed on the front surface of specimen .The rise of temperature on opposite side of sample is calculated and then thermal diffusivity is evaluated by temperature increase versus time values. The suggested techniques also allows identification of specific heat , thus allowing calculation of thermal conductivity. Thermal diffusivity of specimen is calculated from specimen thickness and time needed for rear surface temperature increase to reach 50% of its highest value ($t_{1/2}$) [101].

$$\alpha = 1.388\frac{d^2}{t_{1/2}\pi^2} \qquad (4.4)$$

where , d is sample thickness and $t_{1/2}$ is time needed for rear surface temperature to reach half of highest temperature rise. The properties of specimen is supposed to remain unchanged during the test because temperature rise of specimen is small. For wide temperature calculation of thermal diffusivity of specimen the process is required to be repeated at each temperature of interest.

In Laser Flash method specimen is opaque disk of 10 or 5mm in diameter and 0.5mm to 3mm in thickness, and glazed with a graphite spray for improving assimilation of Xenon light pulse and discharge of IR radiation to temperature indicator. Specimen is placed on a sample bot , situated in a furnace. Specimen is further heated in a furnace at certain temperature. Computed energy pulse is used for illuminating sample surface. Uniform temperature rise takes place on sample surface because of energy pulse. Below shows the schematic diagram and photo of the Laser Flash Technique installed at NPL

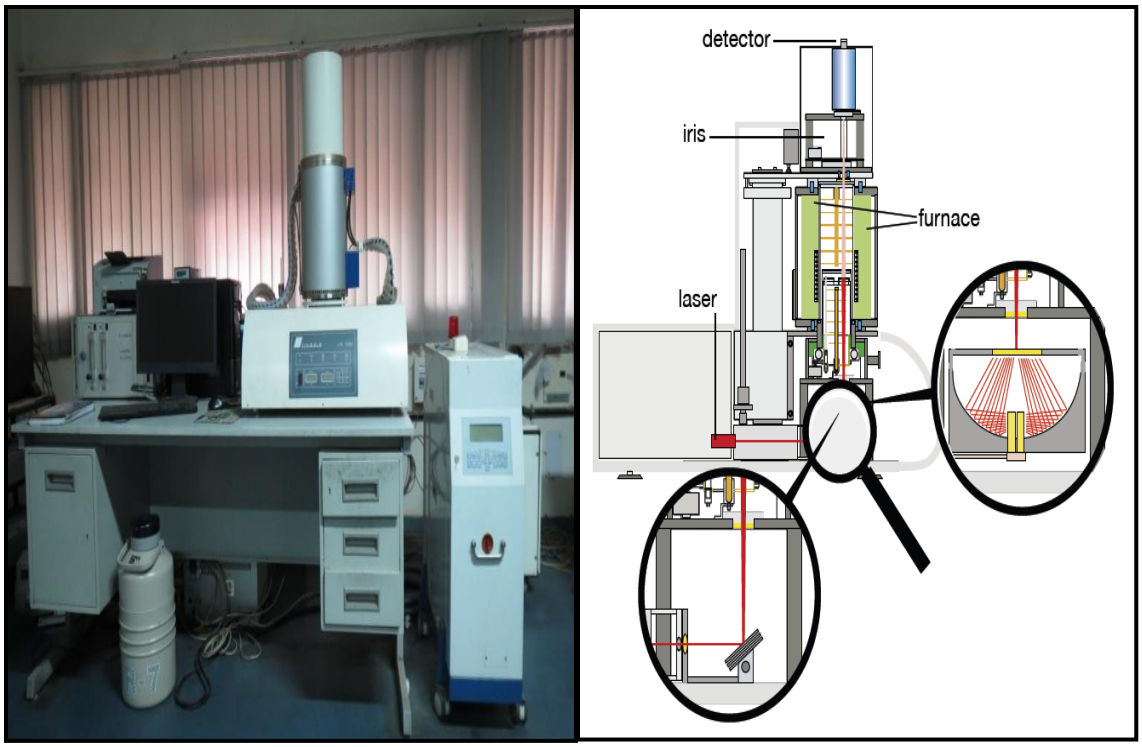

Figure 4.11 Laser Flash Method Setup at NPL

4.7 Seebeck Coefficient Measurement System

Seebeck Coefficient of a material determines magnitude of an induced thermoelectric voltage in respond to temperature difference across the material. Seebeck Coefficient ,electrical conductivity of the specimen has been measured by instrument Make, ULVAC-RIKO(JAPAN)Model:ZEM-3. For the Seebeck Coefficent measurements the specimen has cuboids shape with dimension (2 x 2 x 10 mm) and vertically positioned between two electrodes as shown in the figure below. The lower electrode block contains a heater.

When the lower block heated the lower part of the specimen also heated at specified temperatures which provide a temperature gradient to the specimen. Seebeck Coefficient is measured by measuring the upper and lower temperatures T1 and T2 with the thermocouples pressed against the side of the sample ,followed by measurement of thermal electromotive force dE between the same wires. Complete setup of measurement is placed in furnace. Sample is heated to a certain temperature by the help of furnace

surrounding measurement setup. Lower electrode block generates a temperature difference.

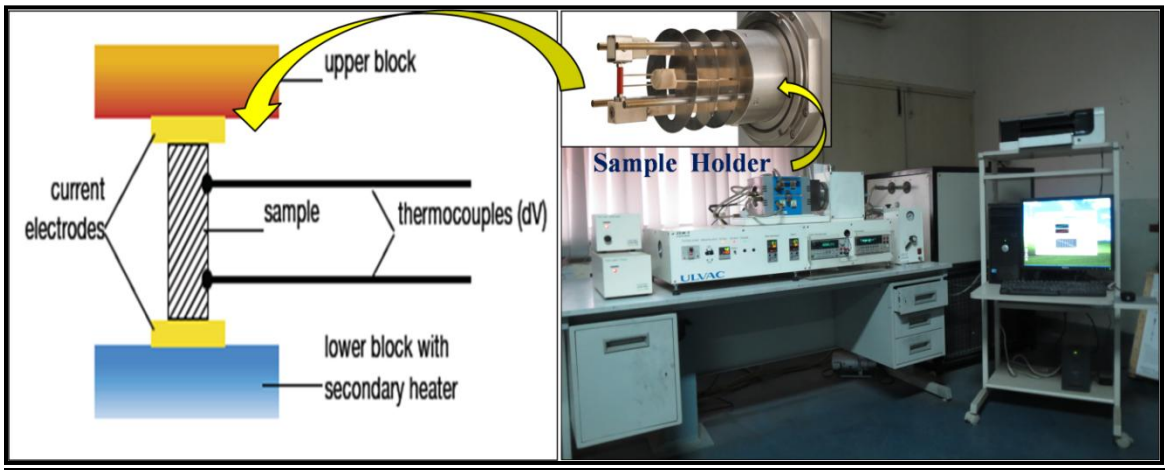

Figure 4.12 Seebeck Coefficient Measurement Setup at NPL.

Seebeck Coefficient of the MWCNTs reinforced bismuth telluride composite were determined by this techniques.

CHAPTER 5
Result & Discussion

5.1 Characterization of 1.5% by weight CNT reinforced Bi_2Te_3

5.1.1 XRD Analysis

XRD pattern shown above in figure 5.1 indicates that VDS grown Bismuth Telluride that was used is single phase having rhombohedral structure of Bi_2Te_3. The lattice parameters from XRD data are compared with standard data of JCPDS 15-0863. Crystallite size of each crystal Plane was calculated by using Scherrer Formula given below:

$$\beta = \frac{k\lambda}{t\cos\theta}$$

where , β is peak width, t is crystallite size and λ is X-ray wavelength.

Value of elastic strain also calculated in each crystal by using formula given below:

$$\beta = \frac{-2\varepsilon}{Cot\theta}$$

where , ε is elastic strain.

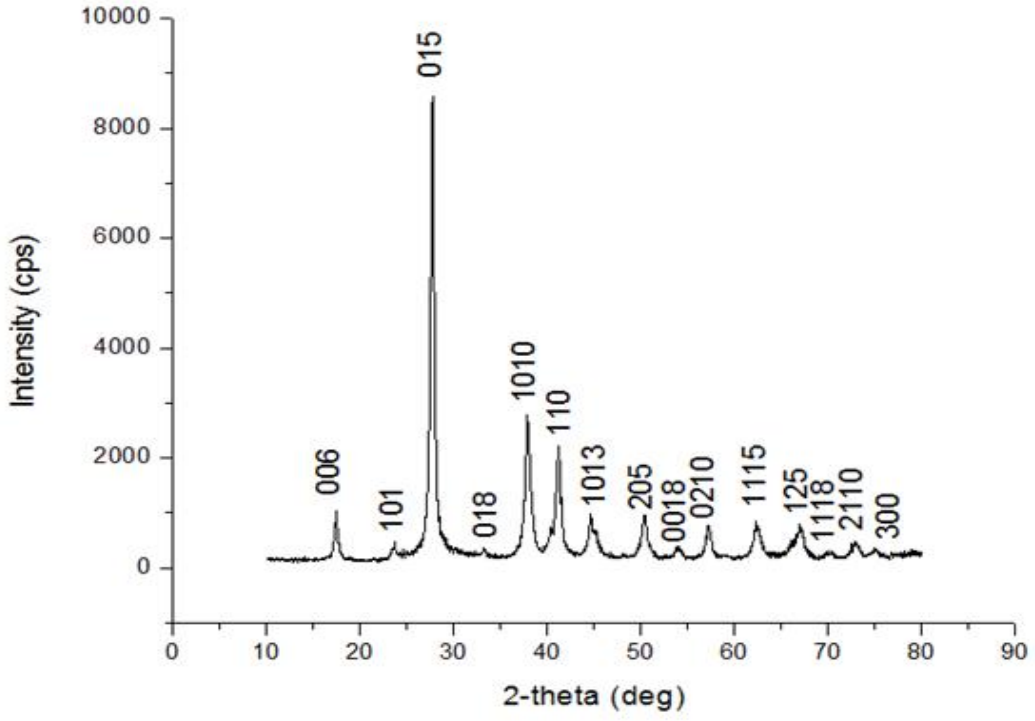

Figure 5.1 XRD pattern of 1.5% by weight CNT reinforced Bi_2Te_3.

Table 5.1 Crystallite size of 1.5% by weight CNT reinforced Bi_2Te_3.

Crystal Plane	**(006)**	**(015)**	**(1010)**	**(110)**	**(205)**	**(0210)**	**(1115)**	**(125)**
Crystallite Size(nm)	**15.264**	**15.625**	**11.805**	**11.781**	**14.125**	**15.190**	**12.068**	**13.576**

Table 5.2 d-spacing of 1.5% by weight CNT reinforced Bi_2Te_3.

Crystal Plane	**(006)**	**(015)**	**(1010)**	**(110)**	**(205)**	**(0210)**	**(1115)**	**(125)**
d-spacing (nm)	**5.084**	**3.216**	**2.371**	**2.187**	**1.811**	**1.608**	**1.488**	**1.395**

Table 5.3 Elastic strain of 1.5% by weight CNT reinforced Bi_2Te_3.

Crystal Plane	**(006)**	**(015)**	**(1010)**	**(110)**	**(205)**	**(0210)**	**(1115)**	**(125)**
Elastic Strain	**0.029**	**0.018**	**0.018**	**0.016**	**0.011**	**0.009**	**0.011**	**0.009**

Crystallite size, d-spacing and elastic strain of each crystal planes shown in the above tables. It was clear from the table that the crystallite size varied between 11.781nm to 15.625nm.Value of d-spacing exist between 1.395 nm to 5.084 nm. Value of Elastic strain exist between 0.029 to 0.009.

5.1.2 SEM Analysis

In Figure 5.2 SEM images of the powder of 1.5% by weight CNT reinforced Bi_2Te_3 after ultrasonication for 90 minutes and then Ball Milled for 1hour. The images clearly show the presence of MWCNTs in the powder. From images it was observed that the particle size was around 1μm. Some fine particles of size less than 1μm were also seen in the micrograph.

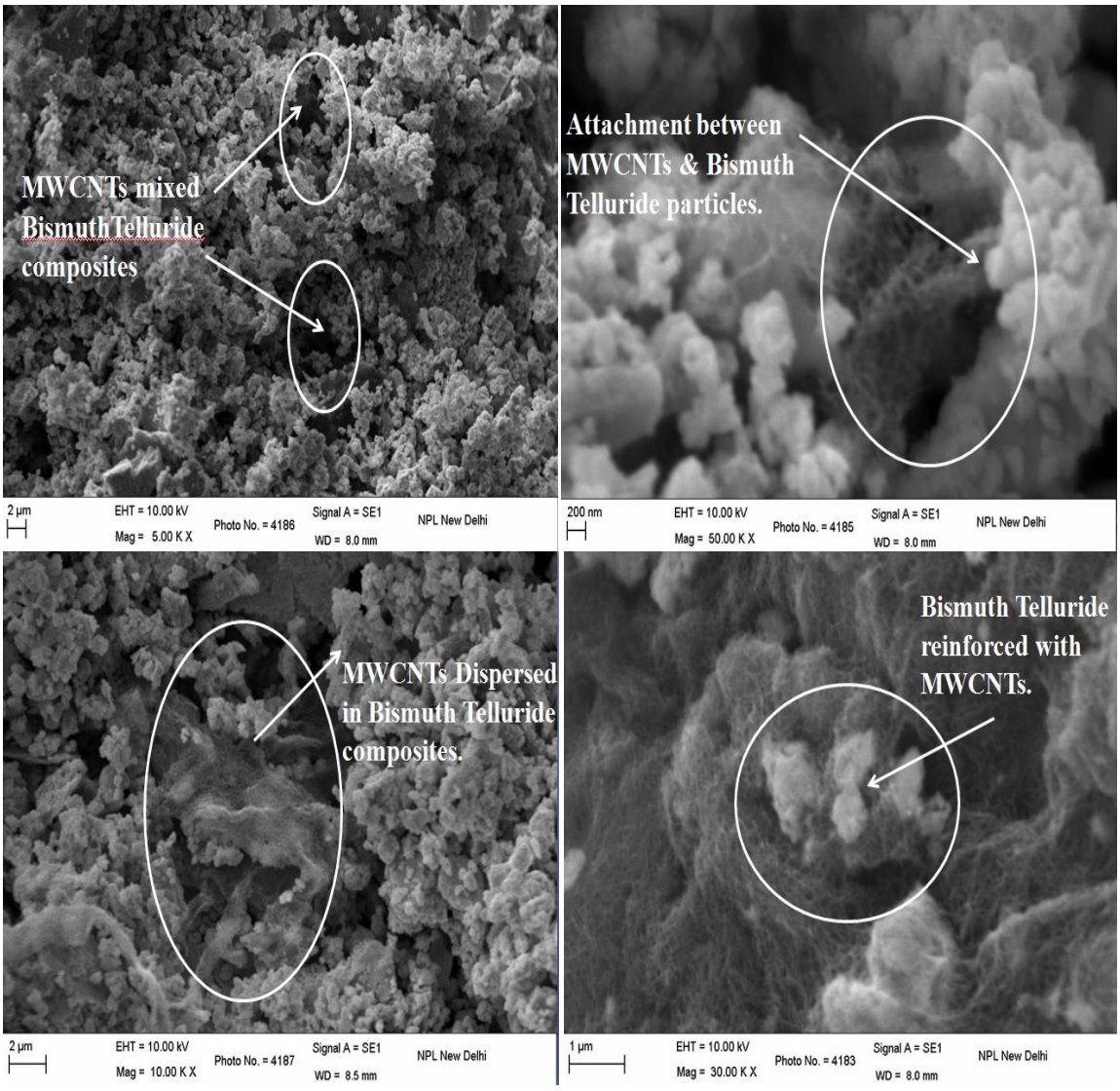

Figure 5.2 SEM images of 1.5% by weight CNT reinforced Bi_2Te_3.

5.1.3 EDS Spectra

From EDS spectra shown above in the figure 5.3 it was observed that the stoichiometry of Bi_2Te_3 was maintained. Peaks of Bismuth and Telluride were obtained in spectra. Peak of Carbon confirmed the presence of MWCNTs in the sample.

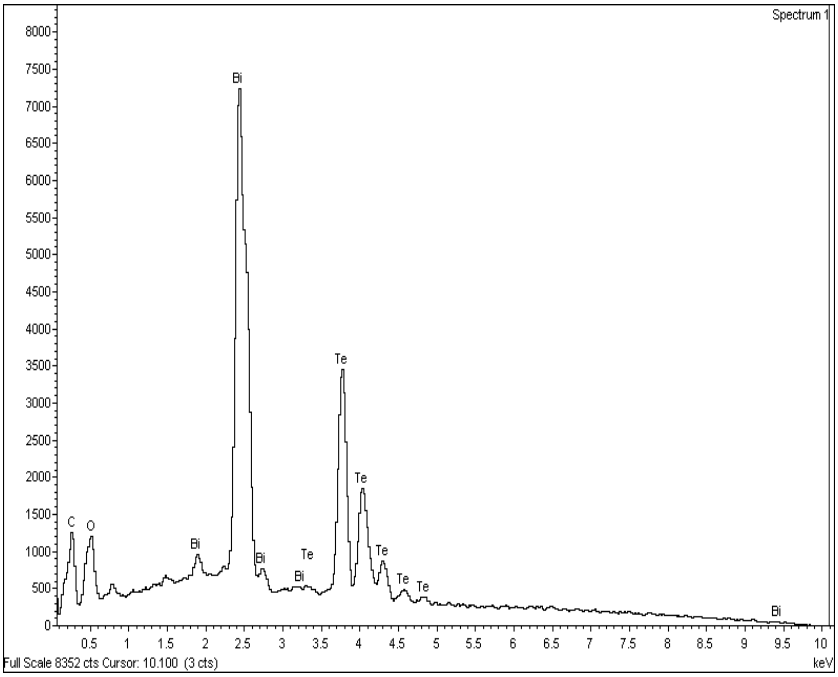

Element	Weight%	Atomic%
C	2.36	21.39
O	1.97	13.44
Te	45.82	39.16
Bi	49.85	26.01
Total	100.0	

Figure 5.3 EDS Spectra of 1.5% by weight CNT reinforced Bi_2Te_3.

5.1.4 HRTEM Analysis

Microstructural features of 1.5% by weight CNT reinforced Bi_2Te_3 powder ball milled for 1hour was recorded by using HRTEM operated at 300kV. From various TEM images it was observed that the particle size after ball milling for 1hour was 100 nanometer.

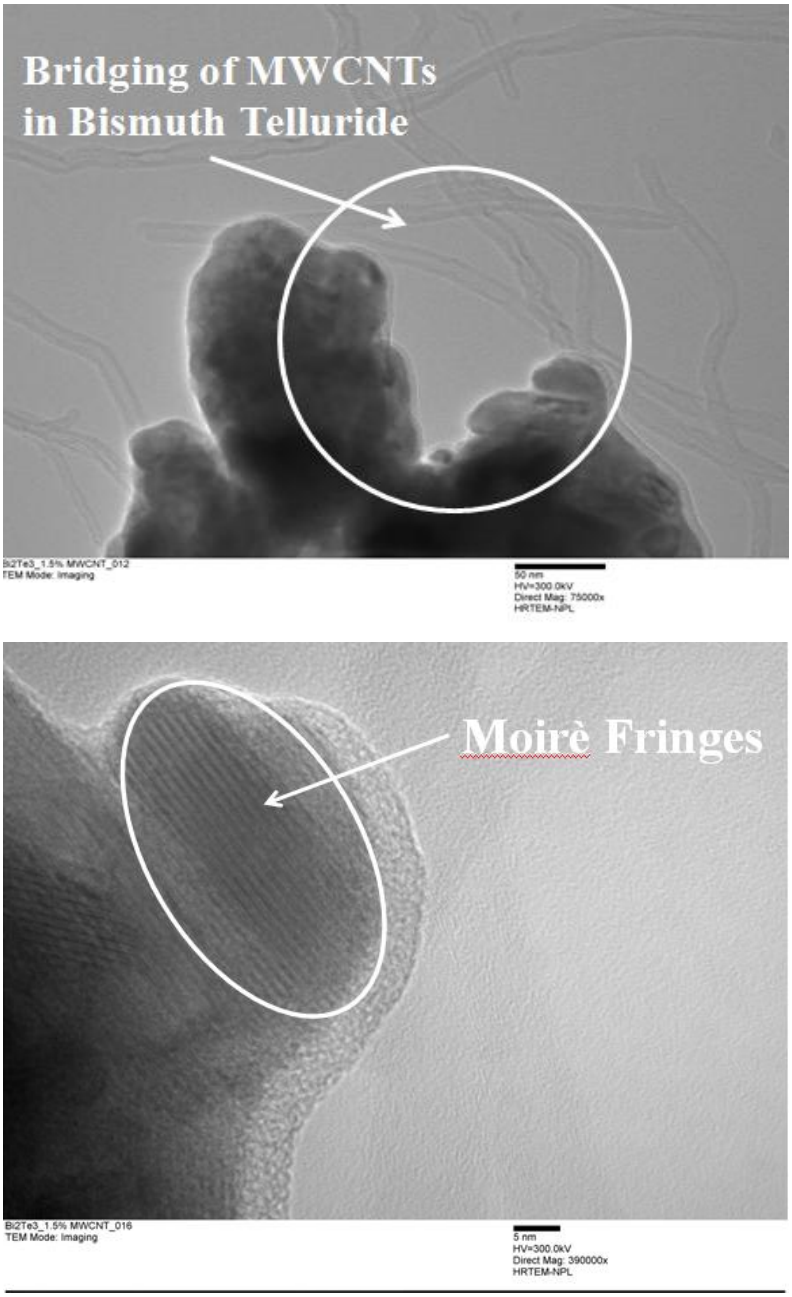

Figure 5.4 HRTEM images of 1.5% by weight CNT reinforced Bi_2Te_3.

TEM images recorded at higher magnification in which MWCNTs were seen throughout the area. In images the proper bridging and entangling of MWCNTs with Bi_2Te_3 nanoparticles was observed.

Electron Diffraction Analysis

SAEDP (Selected Area Electron Diffraction Pattern) of the powder of 1.5% by weight CNT reinforced Bi_2Te_3 to find out the presence of Bi_2Te_3 nanoparticles and carbon nanotubes by using diffraction mode in HRTEM. From SAEDP it was observed that the composite was polycrystalline in nature. Reflection of rings in the diffraction pattern when analyzed found to have the presence of bismuth telluride and carbon nanotubes. Some weak rings in diffraction pattern may be due to the development of strains during the ball milling of the composite as depicted in the figure 5.5 below.

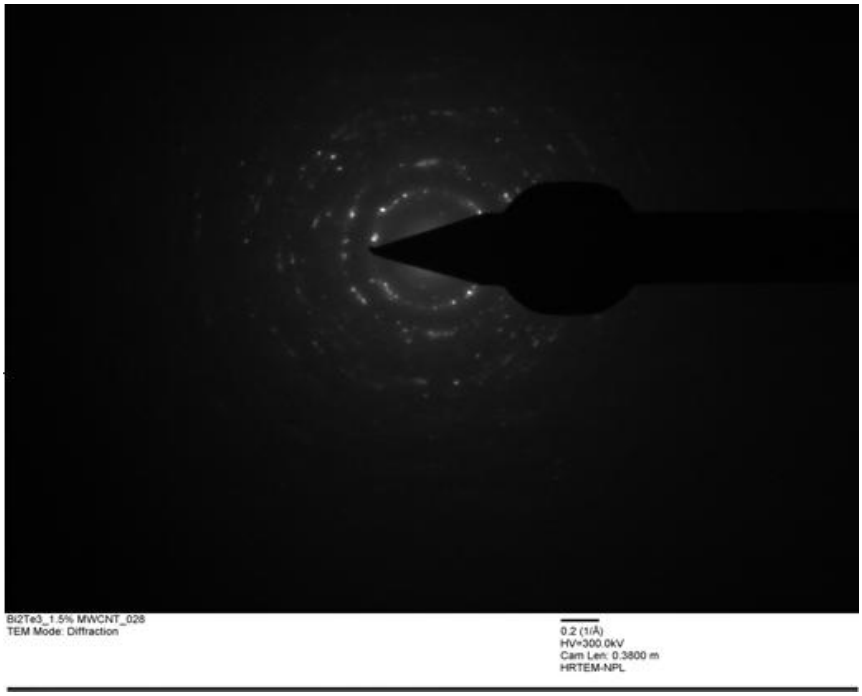

Figure 5.5 SAEDP of 1.5% by weight CNT reinforced Bi_2Te_3.

Formation of the rings was due to the polycrystalline nature of VDS grown Bismuth Telluride. Very weak rings in the diffraction pattern were seen due to stress and the dislocation defects in the material.

5.2 Characterization of 3% by weight CNT reinforced Bi_2Te_3

5.2.1 XRD Analysis

XRD pattern of 3% by weight CNT reinforced Bi_2Te_3 was recorded and reduction in intensity was observed for peaks at (006),(015) and (1010) planes. Plane (125) was completely vanished because of development of stress and strain during the ball milling process and new peak was observed at (0120) plane because of the presence of MWCNTs in the nanocomposite.

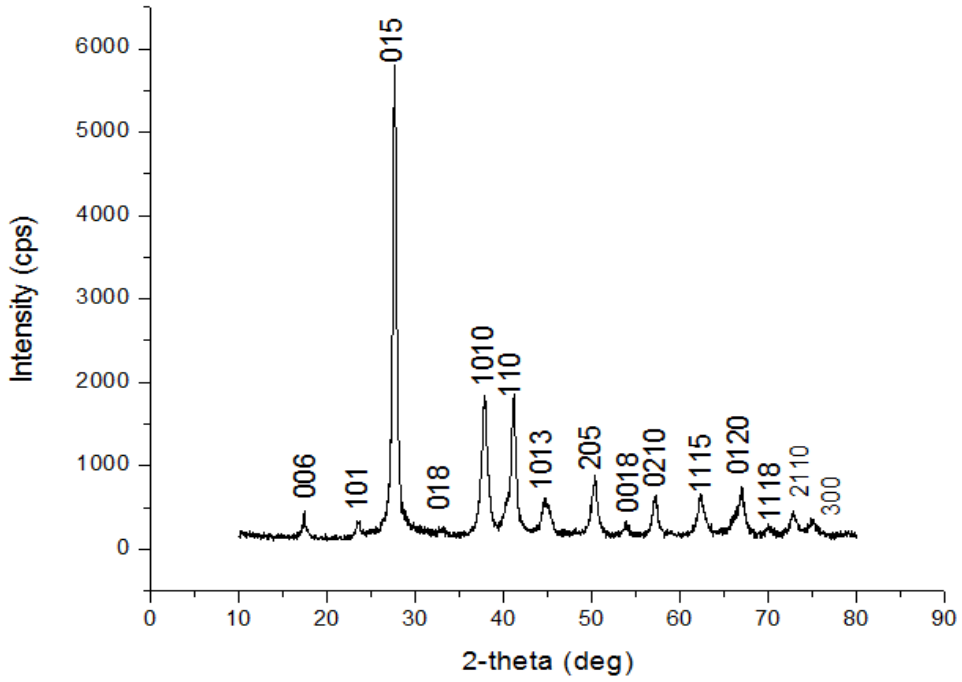

Figure 5.6 XRD pattern of 3% by weight CNT reinforced Bi_2Te_3.

Crystallite size of each crystal plane was calculated by using well known scherrer formula. Crystallite size of each crystal plane given in the following table. Crystallite size value exist between 12.192nm to 26.994nm.d-spacing of each crystal plane was calculated using Bragg's law and its values were mentioned in table 5.5. d - spacing value exist between 1.397 nm to 5.084 nm.

Table 5.4 Crystallite size of 3% by weight CNT reinforced Bi_2Te_3.

Crystal Plane	**006**	**015**	**1010**	**110**	**205**	**0210**	**1115**	**0120**
Crystallite Size(nm)	**26.994**	**15.944**	**12.192**	**15.950**	**12.800**	**15.745**	**12.051**	**15.472**

Table 5.5 d - spacing of 3% by weight CNT reinforced Bi_2Te_3.

Crystal Plane	**006**	**015**	**1010**	**110**	**205**	**0210**	**1115**	**0120**
d-spacing (nm)	**5.084**	**3.225**	**2.373**	**2.191**	**1.811**	**1.608**	**1.489**	**1.397**

Table 5.6 Elastic strain of 3% by weight CNT reinforced Bi_2Te_3.

Crystal Plane	**006**	**015**	**1010**	**110**	**205**	**0210**	**1115**	**0120**
Elastic Strain	**0.016**	**0.018**	**0.017**	**0.012**	**0.023**	**0.009**	**0.011**	**0.013**

Elastic strain in each crystal plane was also calculated .Elastic strain in each crystal plane given in table 5.6 Elastic strain value in each crystal plane varied between 0.009 to 0.023.Elastic strain was introduced due to the breaking of CNTs because of ball milling.

5.2.2 SEM Analysis

SEM images of 3% by weight CNT reinforced Bi_2Te_3 clearly indicates the presence of MWCNTs. From the above shown SEM images it was observed that particle size of Bismuth telluride was around 1μm.Some fine particles were also seen in images of particle size less than 1μm.

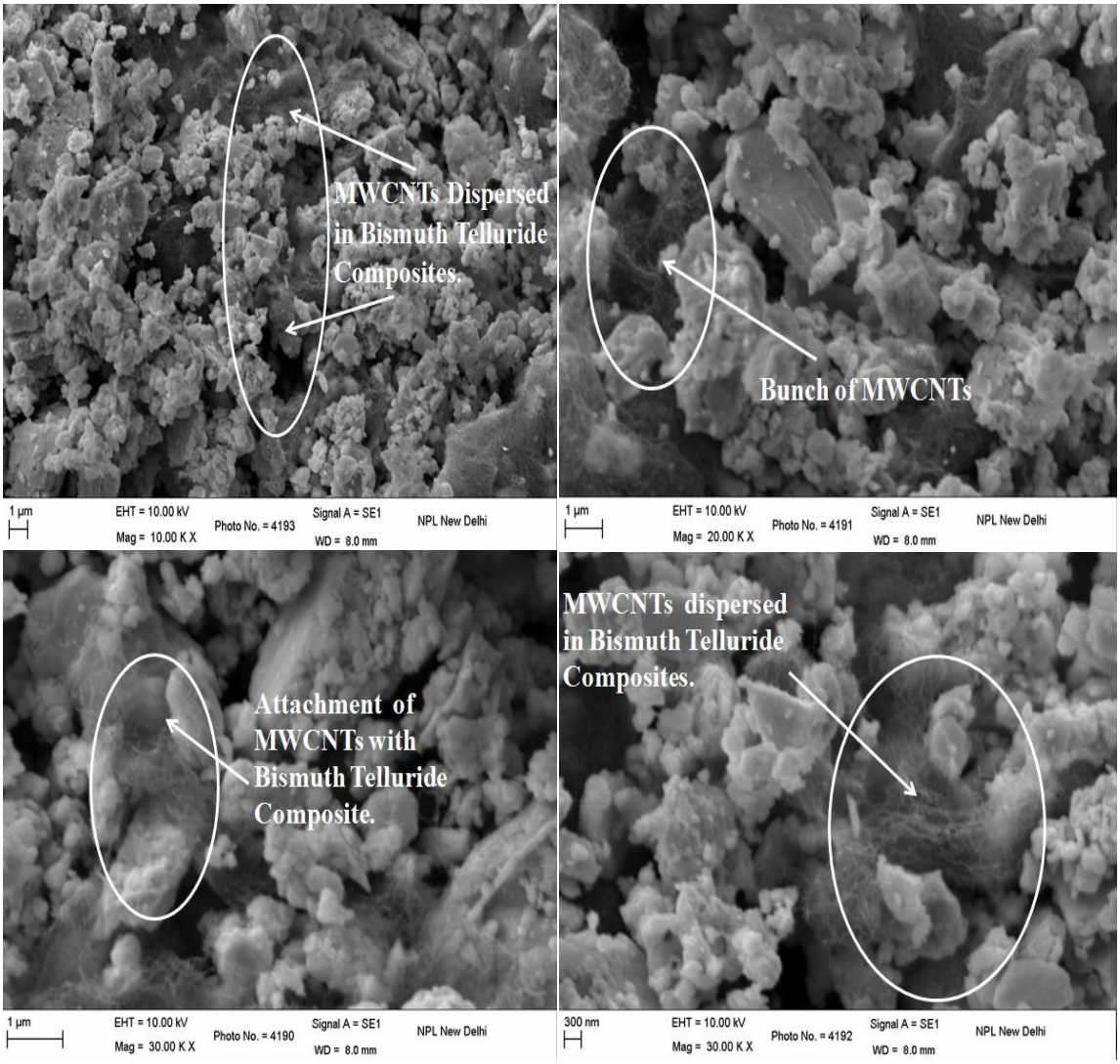

Figure 5.7 SEM images of 3% by weight CNT reinforced Bi_2Te_3.

5.2.3 EDS Spectra

From EDS spectra shown above in the figure 5.8 it was observed that the stoichiometry of Bi_2Te_3 was maintained. Peaks of Bismuth and Telluride obtained in spectra. Peak of Carbon confirmed the presence of MWCNTs in the sample.

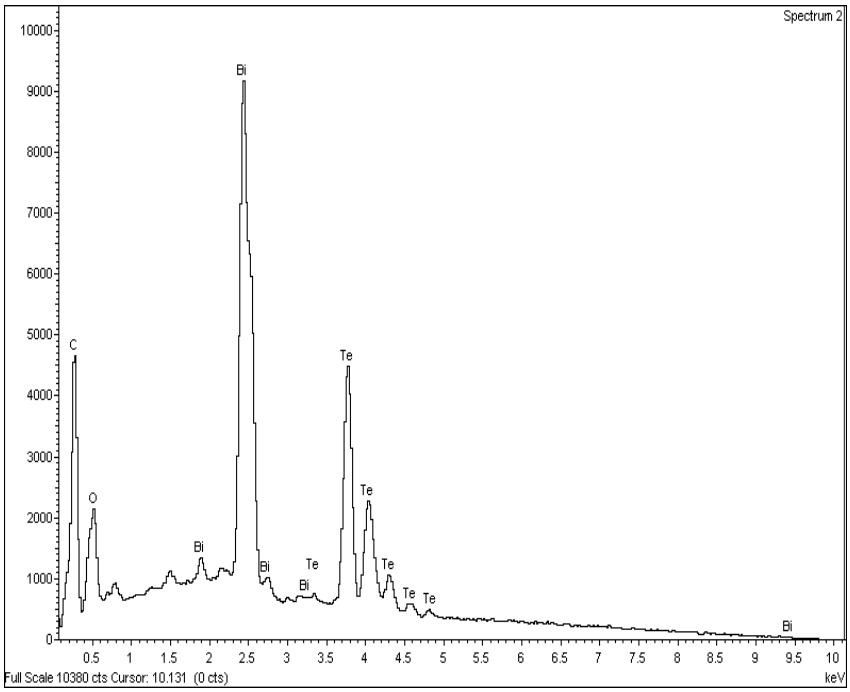

Element	Weight%	Atomic%
C	8.15	47.97
O	2.88	12.75
Te	42.46	23.54
Bi	46.51	15.74
Total	100.0	

Figure 5.8 EDS Spectra of 3% by weight CNT reinforced Bi_2Te_3.

5.2.4 HRTEM Analysis

Microstructural features of 3% by weight CNT reinforced Bi_2Te_3 powder ball milled for 1 hour was recorded by using HRTEM operated at 300kV. From various TEM images it was observed that the particle size after ball milling for 1 hour reduced to 100 nanometer. TEM images recorded at higher magnification in which MWCNTs were seen throughout the area. In images the proper bridging and entangling of MWCNTs with Bi_2Te_3 nanoparticles was observed.

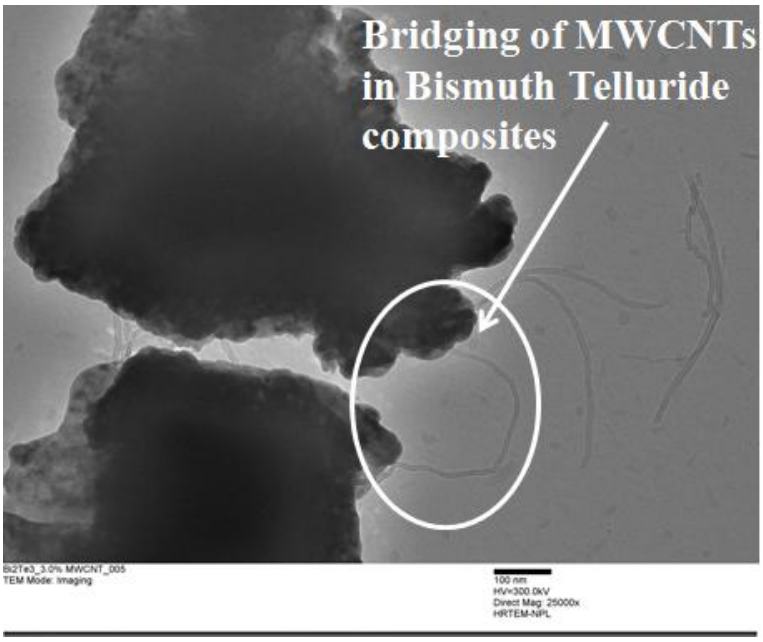

Figure 5.9 HRTEM images of 3% by weight CNT reinforced Bi_2Te_3.

Electron Diffraction Analysis

SAEDP (Selected Area Electron Diffraction Pattern) of the powder of 3% by weight CNT doped Bi_2Te_3 to find out the presence of Bi_2Te_3 nanoparticles and carbon nanotubes by using diffraction mode in HRTEM. From SAEDP it was observed that the composite was polycrystalline in nature. Reflection of rings in the diffraction pattern when analyzed found to have the presence of bismuth telluride and carbon nanotubes.

Some weak rings in diffraction pattern because of the development of strains during the ball milling of the composite as depicted in the figure 5.10 below.

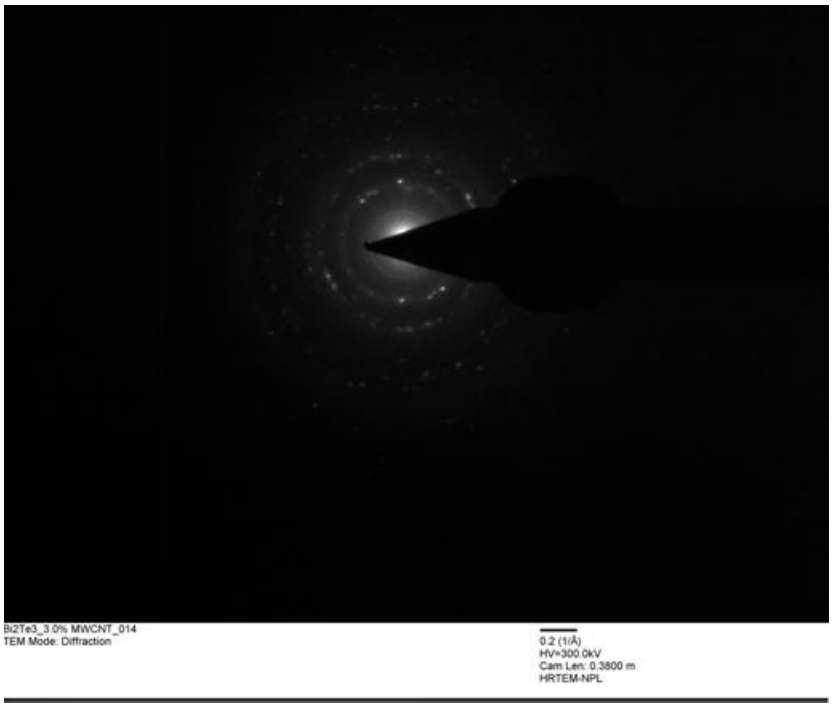

Figure 5.10 SAEDP of 3% by weight CNT reinforced Bi_2Te_3.

Formation of the rings was due to the polycrystalline nature of VDS grown Bismuth Telluride. Very weak rings in the diffraction pattern were seen due to stress and the dislocation defects in the material.

5.3 Raman Spectrum

Raman spectroscopy is mainly used for investigating structural and physical properties of CNTs. Its spectrum provide information related to vibration and electronic properties of materials and mechanical deformation of CNTs.

In Raman spectrum there was decline in the intensity of peak of G-band of CNT(Graphite band defect free) and also decline in intensity of peak of D-band(defective CNT) due to

ball milling. Decrease in G-Band intensity is mainly due to defects in CNTs caused by ball milling and reduction in D-Band intensity represent complete destruction of CNTs.

Raman spectra measurements of CNTs doped bismuth telluride were performed. In raman spectra of 1.5% CNT reinforced Bi_2Te_3 shown in figure 5.11 three peaks were obtained at $89cm^{-1}$,$113cm^{-1}$ and $136cm^{-1}$. It almost matches with the earlier reported values of peaks of bismuth telluride raman spectra. Highest intensity peak was observed at $114cm^{-1}$ and broadening of intensity of peak represent crystallite structure of compound.

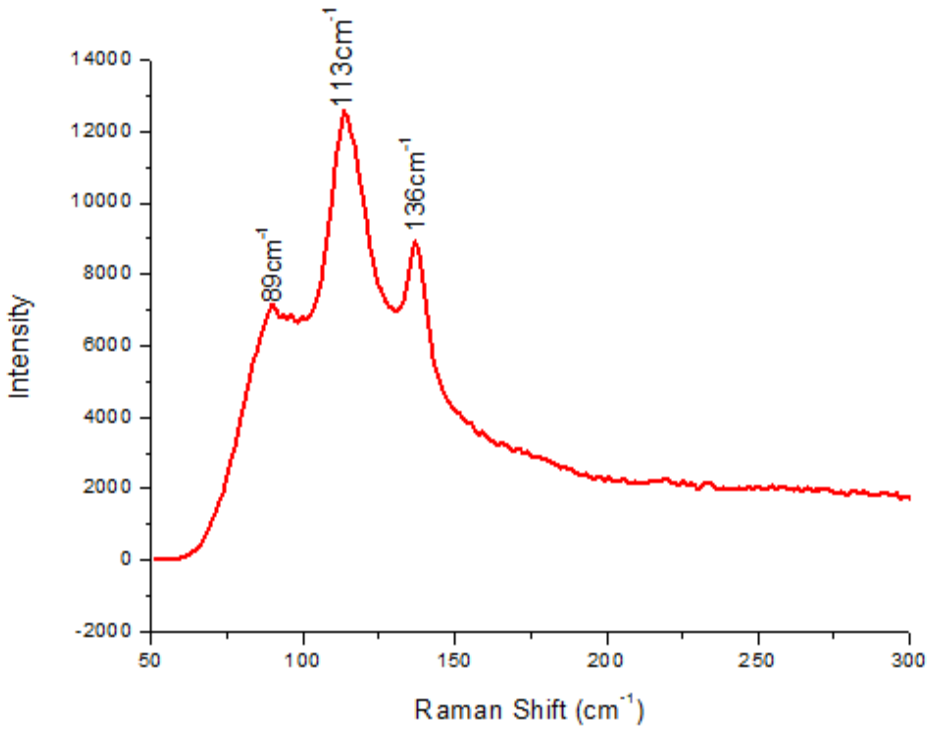

Figure 5.11 Raman Spectra of 1.5% CNT reinforced Bi_2Te_3 in spectrum range of 50 to 300 cm^{-1}.

In 1.5% by weight CNT reinforced Bi_2Te_3 two peaks were recorded in its raman spectra. Peak at 1346cm^{-1} corresponds to D-band (defect mode), peak observed at 1579cm^{-1} corresponds to G-band (related to tangential vibrations of carbon atoms.) Presence of peaks in raman spectra authenticate the presence of MWCNTs.

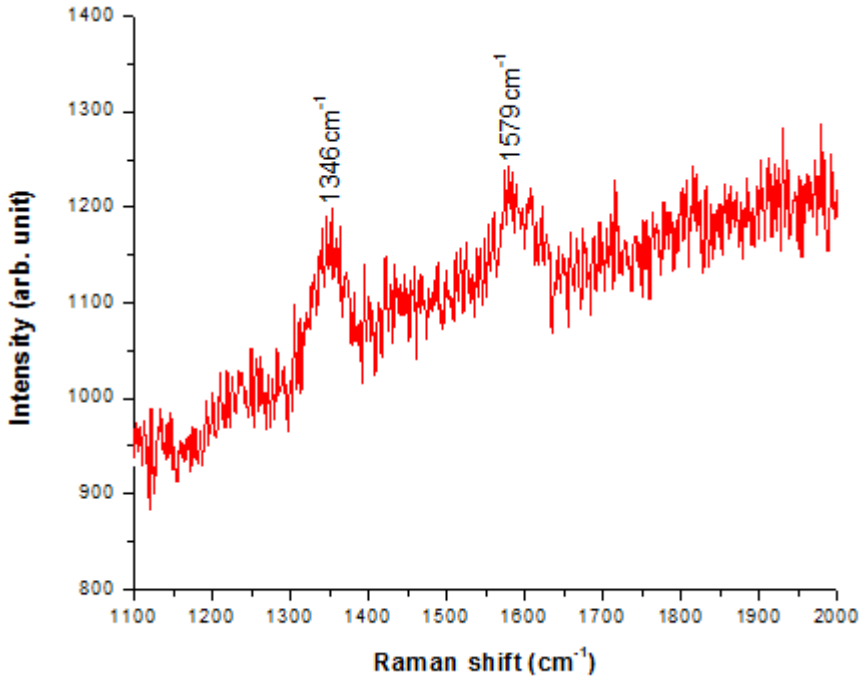

Figure 5.12 Raman Spectra of 1.5% by weight CNT reinforced Bi_2Te_3.

In raman spectra of 3% by weight CNT reinforced Bi_2Te_3 three peaks were obtained at $89cm^{-1}$,$114cm^{-1}$ and $138cm^{-1}$. It almost matches with the reported value of peaks of bismuth telluride. Highest intensity peak was obtained at $114cm^{-1}$. Broadening of peaks at $114cm^{-1}$ represents crystallite structure of material.

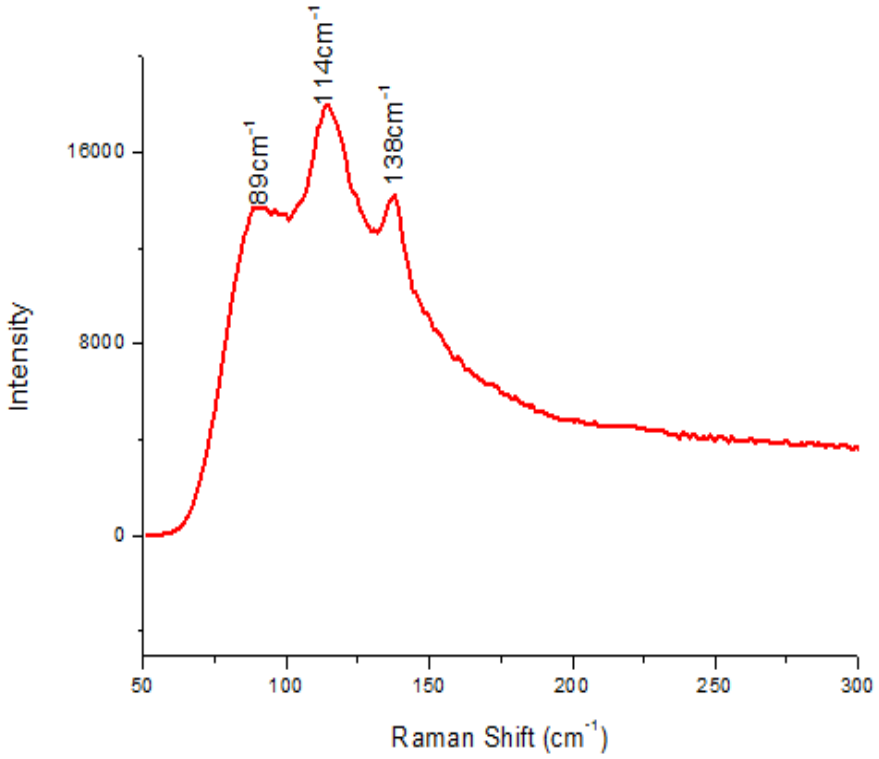

Figure 5.13 Raman Spectra of 3% CNT reinforced Bi_2Te_3 in spectrum range of 50 to 300 cm^{-1}.

In 3% by weight CNT reinforced Bi_2Te_3 raman spectra two peaks were obtained which represents D-band and G-band respectively. Peak obtained at 1345cm^{-1} represent D-band and other peak obtained at 1585cm^{-1} represent G-band. Intensity of peak at 1345cm^{-1} was higher than the peak at 1585cm^{-1}.

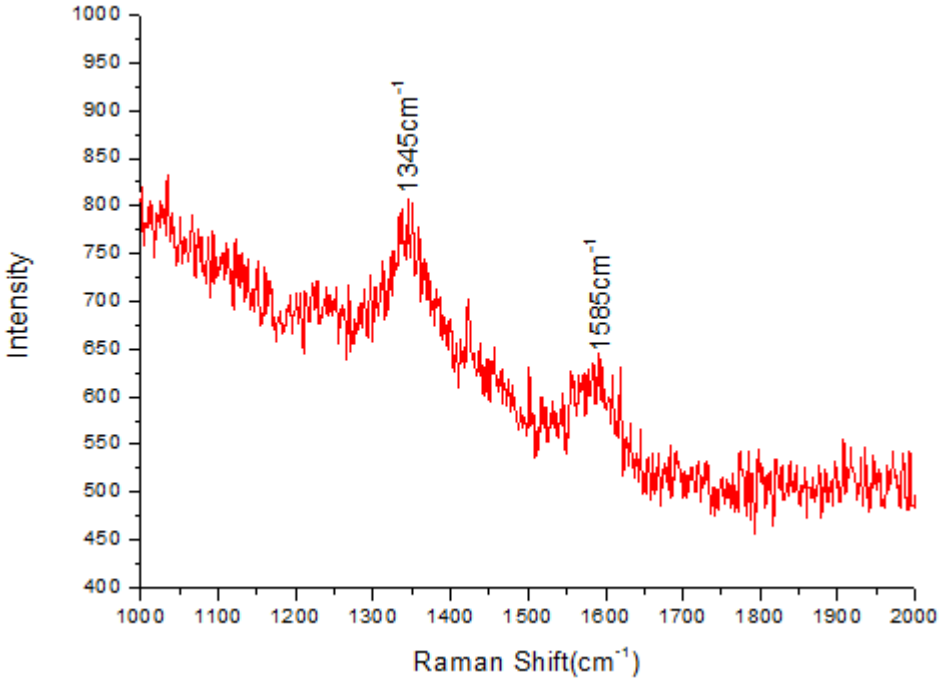

Figure 5.14 Raman Spectra of 3% by weight CNT reinforced Bi_2Te_3.

5.4 Determination of Thermoelectric Parameters

5.4.1 Thermal Conductivity Measurement

1.5% by weight CNT reinforced Bi_2Te_3 Nanocomposite

Thermal Conductivity of the nanocomposite calculated by using Laser Flash Method. Thermal Conductivity of 1.5% by weight CNT reinforced Bi_2Te_3 remains constant in beginning then its value starts decreasing and reaches minima .After achieving minima its value again starts increasing and reaches maxima. The decrease in value of thermal conductivity is favourable for our purpose of achieving higher value of ZT.

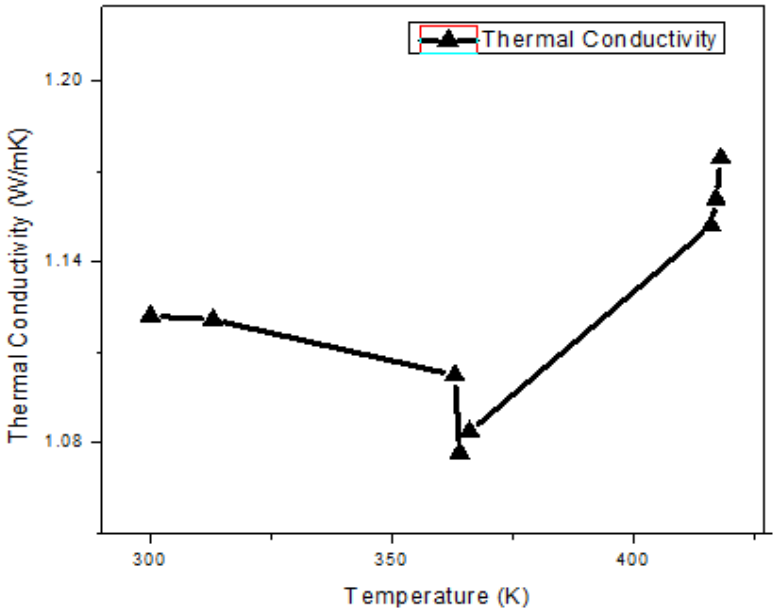

Figure 5.15 Variation Of Thermal Conductivity with Temperature of 1.5% by weight CNT reinforced Bi_2Te_3 Nanocomposite.

3% by weight CNT reinforced Bi_2Te_3 Nanocomposite

Thermal conductivity of 3% by weight CNT reinforced Bi_2Te_3 decreases with rise in temperature. As the temperature increases thermal conductivity reaches its minima. Further rise in temperature results in increment of the value of thermal conductivity. The value of thermal conductivity decreases with increase in amount of CNT reinforcement. Presence of CNT in bismuth telluride composites creates more interfaces, defects and improve density of grain boundaries.Due to which phonon scattering at interfaces of grain boundaries takes place which were responsible for reduction in value of thermal conductivity.

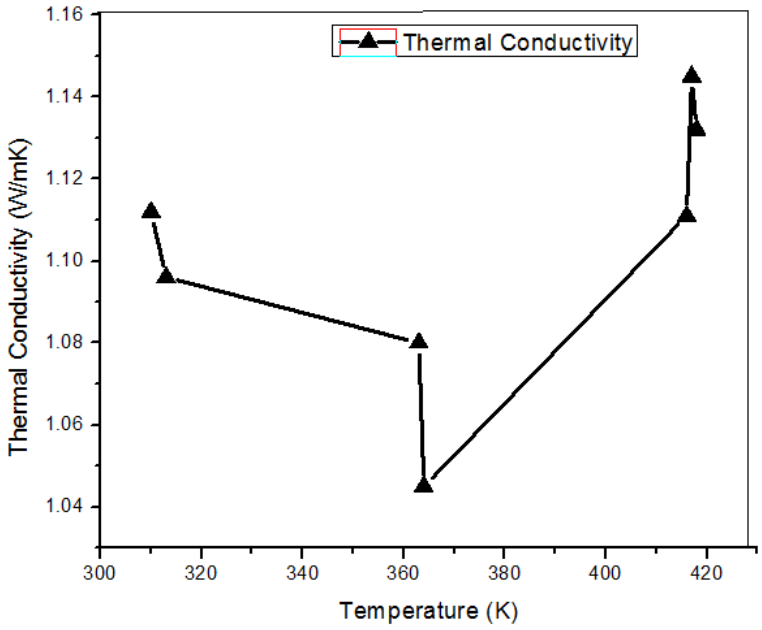

Figure 5.16 Variation Of Thermal Conductivity with Temperature of 3% by weight CNT reinforced Bi_2Te_3 Nanocomposite.

In both the samples for certain range of temperature it was possible to reduce the value of thermal conductivity which contributes in achieving higher value of figure of merit.

5.4.2 Seebeck's Coefficient Measurement

1.5% by weight CNT reinforced Bi_2Te_3 Nanocomposite

Seebeck's coefficient of 1.5% by weight CNT reinforced Bi_2Te_3 increases with increase in value of temperature. Seebeck's coefficient increases steadily with increase in temperature. Higher value of Seebeck's coefficient required for improving the figure of merit. In this sample the increment in value of seebeck's coefficient , a good indication towards improvement of thermoelectric efficiency.

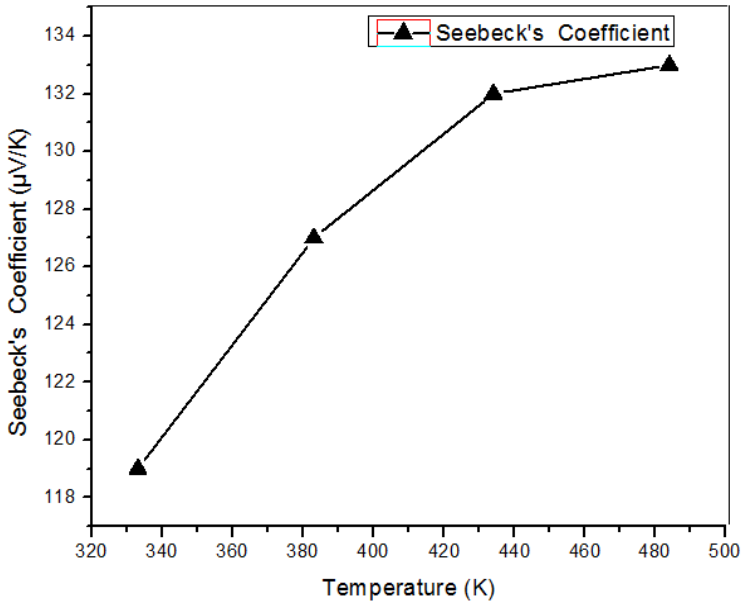

Figure 5.17 Variation Of Seebeck's Coefficient with Temperature of 1.5% by weight CNT reinforced Bi_2Te_3 Nanocomposite.

3% by weight CNT reinforced Bi_2Te_3 Nanocomposite

Seebeck's coefficient of 3% by weight CNT reinforced Bi_2Te_3 increases initially with increase in temperature. Seebeck's coefficient after achieving maxima, the value of seebeck's coefficient starts decreasing with rise in temperature. Seebeck's coefficient with higher value is favourable while lower value of seebeck's coefficient at higher temperature will results in lowering the value of figure of merit.

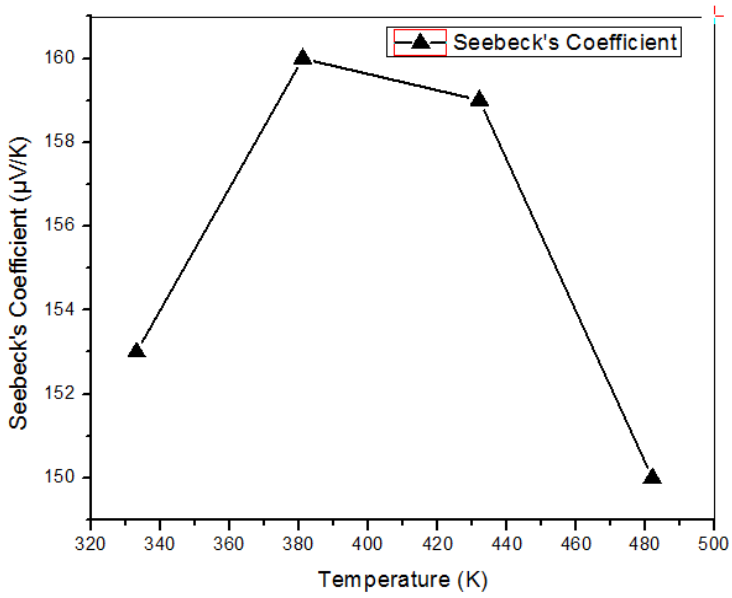

Figure 5.18 Variation Of Seebeck's Coefficient with Temperature of 3% by weight CNT reinforced Bi_2Te_3 Nanocomposite.

In both samples there exist a range of temperature in which it is possible to achieve higher value of seebeck's coefficient which will contribute in purpose of improving value of figure of merit. In 3% by weight CNT doped reduction in value of Seebeck's coefficient may be due to the large amount of CNTs present in the sample.

5.4.3 Electrical Conductivity Measurement

1.5% by weight CNT reinforced Bi_2Te_3 Nanocomposite

Electrical conductivity of 1.5% by weight CNT reinforced Bi_2Te_3 decreases with rise in temperature. At high temperature low value of electrical conductivity represents the metallic property of bismuth telluride. Since in metals with increase in temperature the mobility of electron decreases which results in the reduction of electrical conductivity.

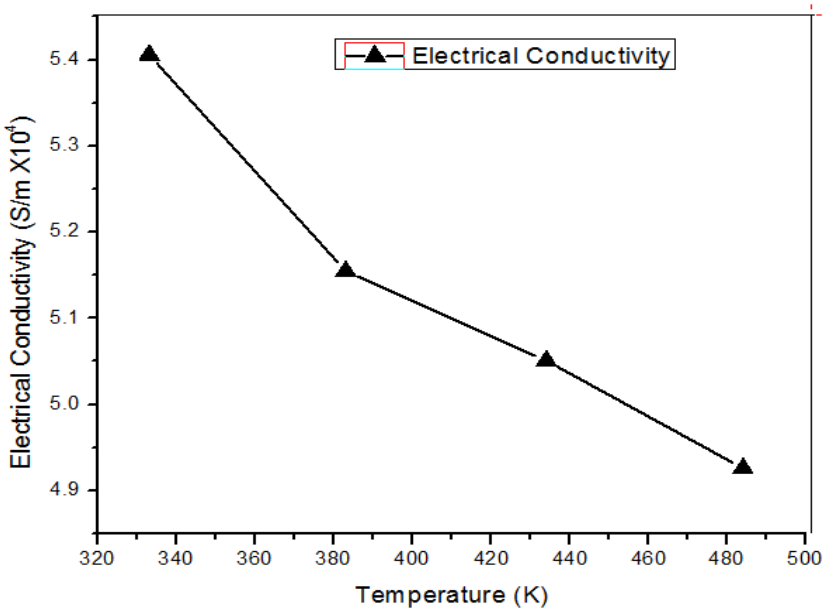

Figure 5.19 Variation Of Electrical Conductivity with Temperature of 1.5% by weight CNT reinforced Bi_2Te_3 Nanocomposite.

.

Decrease in value of electrical conductivity may be due to non uniform distribution of CNTs in bismuth telluride composite.

3% by weight CNT reinforced Bi_2Te_3 Nanocomposite

Electrical conductivity of 3% by weight CNT reinforced Bi_2Te_3 is higher than that of 1.5% by weight CNT reinforced Bi_2Te_3. The reason behind higher value of electrical conductivity may be the higher concentration CNTs in it. The value of electrical conductivity decreases with increase in temperature represent its metallic property. The reduction in electrical conductivity may be due to irregular dispersion of CNTs in composite.

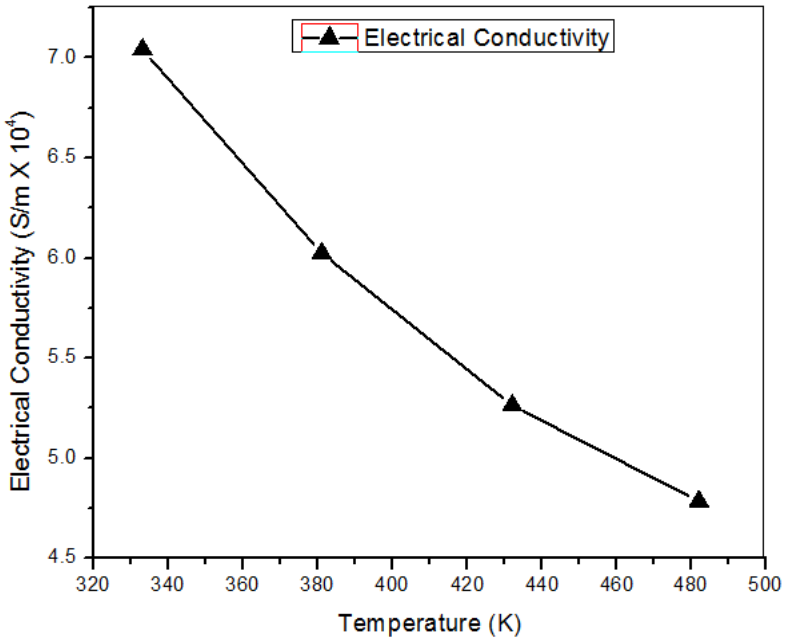

Figure 5.20 Variation Of Electrical Conductivity with Temperature of 3% by weight CNT reinforced Bi_2Te_3 Nanocomposite.

The value of figure of merit (ZT) is calculated for both samples from thermoelectric parameters obtained by Laser Flash technique. Value of ZT is higher in the samples containing higher amount of CNTs which indicates that addition of CNTs in bismuth telluride composites will improve value of ZT. For 3% CNT doped Bi_2Te_3 calculated value of ZT is 0.58 at 381°K and for 1.5% CNT doped Bi_2Te_3 calculated value of ZT is 0.42 at 484°K

Table 5.7 Shows the thermoelectric parameters for ball milled nanostructured Bi_2Te_3. (Earlier work)

Materials	**Ball milling time BPR**	**SPS Temp/Pressure**	**Electrical. Cond.** (S/m)	**Seebeck Coeff.** (μV/K)	**Thermal Cond.**	**Max. Figure of merit (ZT)**
Bi_2Te_3	4hrs (15:1BPR)	673K/6.5kN/m^2	1.08x10^5	-131	1.21	0.72(473K)
Bi_2Te_3	**8hrs (15:1BPR)**	**673K/6.5kN/m^2**	**0.98x10^5**	**-140**	**0.97**	**0.94(473K)**
Bi_2Te_3	12hrs(15:1BPR)	673K/6.5kN/m^2	0.90x10^5	-141	1.02	0.83(473K)

Table 5.8 Shows the thermoelectric parameters for ball milled nanostructured Bi_2Te_3 reinforced with CNTs

Materials	**Ball milling time BPR**	**SPS Temp/Pressure**	**Electrical. Cond.** (S/m)	**Seebeck Coeff.** (μV/K)	**Thermal Cond.**	**Max. Figure of merit (ZT)**
Reinforced 3% CNTs with Bi_2Te_3	**8hrs (15:1BPR)**	**673K/6.5kN/m^2**	**0.6x10^5**	**-160**	**1.04**	**0.58(381K)**
Reinforced 1.5% CNTs with Bi_2Te_3	**8hrs (15:1BPR)**	**673K/6.5kN/m^2**	**0.5x10^5**	**-133**	**1.07**	**0.42(434K)**

.

CHAPTER 6

Conclusion

A high purity single crystal Bismuth telluride ingot was synthesized by vertical directional solidification technique. As grown ingot was finely powdered by using mortar and pestle.It was then ball milled for 8hrs in order to reduced particle size further. MWCNTs was mixed with bismuth telluride powder in two different proportions. Two samples of MWCNTs reinforced bismuth telluride composites were prepared ,one contains 1.5% by weight CNTs and other contains 3% by weight CNTs. Both samples were ultrasonicated for 90 minutes for proper mixing of CNTs in bismuth telluride composites. After ultrasonication it was expected that CNTs were properly dispersed in bismuth telluride composites.

Both samples were then investigated by using HRTEM and SEM /EDS techniques. Micrographs were recorded at suitable areas and at suitable magnifications. The images were analyzed properly in order to see the presence of MWCNTs in bismuth telluride nanostructered particles and the natures of reinforcement. EDS analysis of samples clearly shows that stoichiometric compostion of bismuth telluride was maintained and it also indicated presence of CNTs in sample by showing peak of C element in the EDS spectra. HRTEM images of bismuth telluride reinforced with CNTs samples depicted proper bridging between the bismuth telluride particle and CNTs. From SEM images of sample no proper dispersion of CNTs in bismuth telluride composite was seen. However agglomerates of CNTs are seen at various area in the sample. SAEDP of both samples consist of ring patterns indicating polycrystalline nature of the composite. Reflection of rings in the diffraction pattern when analyzed found to have the presence of bismuth telluride and carbon nanotubes. Some weak rings in diffraction pattern may be due to the development of strains during the ball milling

XRD analysis of both the samples was matched with the standard JCPDF file No.15-0863. Peaks obtained in XRD pattern was found to be matching with the standard values. Some peaks intensity show variation in both samples with respect to standard data. Peaks intensity variation occurs because of the ball milling and addition of MWCNTs. Raman Spectra analysis of both sample was done and it shows peak of MWCNTs and Bi_2Te_3 in different spectral range. Shifting of peaks was observed in both samples and shifting of

peaks was found to be in small amount. Raman Spectra of samples confirms the presence of MWCNTs in both the samples.

Spark Plasma Sintering(SPS) technique was used for making pellets of two samples, SPS technique is preferred. By using SPS technique we can control thermal conductivity because in SPS technique grain growth can be controlled. Thermoelectric parameters of bismuth telluride nanocomposite were measured by Laser Flash Method. By Laser Flash Method we obtained values of Seebeck's Coefficient, thermal conductivity, resistivity and power factor. From the obtained values of thermoelectric parameters it is confirmed that addition of MWCNTs in bismuth telluride composites caused change in its magnitude in electrical conductivity and Seebeck's Coefficient.

In previous chapter we discussed the characterization of Bismuth Telluride and MWCNT nanocomposite and found that bismuth telluride particle size was reduced due to ball milling. This reduction of particle size in the nanocomposite affects its thermal conductivity. By decreasing particle size the number of interfaces encountered by the phonons traveling through the composite is increased thereby increases their scattering and thus reduces the thermal conductivity which is favorable for improving figure of merit.

REFERENCES

[1] Lon E. Bell, "Cooling, Heating, Generating power and Recovering Waste Heat with Thermoelectric System" Science 321.(2008).

[2] Sophie L. Benjamin,C. H.(Kees) de Groot,Chitra Gurnani,Andrew L.Hector,Ruomeng Huang,Elena Koukharenko, William Levason and Gillian Reid, "Controlling the nano-structure of Bismuth telluride by selective chemical vapour deposition from a single source precursor. J. Mater. Chem. A 4865-4869 .(2014)

[3] Terry M.Tritt and M.A.Subramanian,"Thermoelectric Materials,Phenomena and Applications:Bird's Eye View.MRS Bulletin,Volume 31(2006)

[4] Michael Constantine Nicolaou,"Thermoelectric Figure of Merit of Degenerate and Nondegenerate Semiconductors",ProQuest.(2009)

[5] Prof.H.Julian Goldsmid , "The Improvement of a Specific Material – Bismuth Telluride",Springer Series in Material Science Vol.121,PP79-97.(2010).

[6] Rupert Gouws and Houston Eilers, "A review on thermoelectric cooling modules: Installation design, performance and efficiency".(2013)

[7] Roberts, R.B."Absolute scale of thermoelectricity". Nature 265 (5591),(1977).

[8] https://dx.doi.org/10.1126%2Fscience.285.5428.703),(https://www.ncbi.nlm.nih.gov/pubmed/10426986).

[9] Th. J. Seebeck "Magnetische Polarisation der Metalleund Erze Durch Temperatur Differenz"Seebeck Biography 1-2.

[10] G. Magnus, Poggendorf's Annalen der Physic 83, p-469, (1851)

[11] (http://www.eng.fsu.edu/~dommelen/quantum/style_a/nt_pelt.html).

[12] Thomson and William ,"On a mechanical theory of thermoelectric currents"(1851).

[13] A.F. Ioffe,"Physics of semiconductors", Academic Press Inc., New York (1960).

[14] D.S. Kim and C.A. Infante Ferreira,"Solar refrigeration options – a state of the art review, International Journal of Refrigeration, pp. 3–15(2008).

[15] Timothy D. Sands ,“ Designing Nanocomposite Thermoelectric Materials”(2005).

[16] N.W. Ashcroft and N.D. Mermin,“Solid State Physics, (Holt, Rinehart, and Winston, New York(1976).

[17] M. V. Vedernikov,E. K. Iordanishvili and A. F. Ioffe,“Origin of modern semiconductor thermoelectric energy conversion”,17th Int. Conf. on Thermoelectrics, vol 1, pp 37–42 (1998).

[18] Suraj Joottu Thiagarajan, Wie Wang and Ronggui yang, Department of mechanical engineering, University of Colorado, Boulder, CO.

[19] Hochbaum Allon, I Chen, Renkun Delgado, Raul Diaz,Liang Wenjie, Garnett Erik, C. Najarian, Mark, MajumdarArun and Yang Peidong,“Enhanced thermoelectric performance of rough silicon and nanowires". Nature 451 (7175): 163–7, (2008).

[20] Yang, J. ,“ICT 2005. 24th International Conference on Thermoelectrics”, p. 170(2005).

[21] Goldsmid, H.J.; Giutronich, J.E.; Kaila, M.M. (1980). “Thermoelectrics: Direct Solar Thermal Energy Conversion”, Solar Energy 24 (5): 435(1980).

[22] (http://www.esrl.noaa.gov/gmd/hats/flask/hcfc.html).

[23] Harman, T. C.; Taylor, Walsh, MP; Laforge, BE (2002). “Quantum dot superlattice thermoelectric materials and devices” Science 297, (5590): 2229–32. (2002).

[24] M.G.Kanatzidis,Chem.Mater.,22,648(2010).

[25] C.H.Kuo,C.S.Hwang,M.S.Jeng,W.S.Su,Y.W.Chou and J.R.Ku,J.Alloy.Comp.,496,68-7(2010).

[26] S.K.Bux,J.P.Fleurial and R.B.Kaner ,Chem.Commun.46,8311(2010).

[27] X.A.Fan,J.Y.Yang,Z.Xie,K.Li,W.Zhu ,X.K.Duan,C.J.Xiao and Q.Q.Zhang J.Phys.D: Appl.Phys.,40,5975(2007)

[28] S.M.Souza,D.M.Triches,C.M.Poffo,J.C.de Lima,T.A.Grandi and R.S. de Biasi,J.Appl Phys.,109.013512(2011).

[29] G.J.Snyder and E.S.Toberer,Nature Materials.,7,105(2008).

[30] M.Takashiri,S.Tanaka,H.Hagino and K.Miyazaki,J.Appl.Phys.,112,084315(2012)

[31] H.Kitagawa,T.Nagamori,T.Tatsuta,T.Kitamura,Y.Shinohara and Y.Noda,Scr.Mater., 49,309(2003).

[32] D.B.Hyun,T.S.Oh,J.S.Hwang,J.D.Shim and N.V.Kolomoets Scr.Mater.,40,49(1999).

[33] S.Miura,Y.Satob,K.Fukuda,K.Nishimura and K.Ikeda,Mater.Sci.Eng.A.,277,244 (2000).

[34] A.Nozue,Y.H.Park and A.Kawasaki,Proc.22nd Int.Conf.on Thermoele.(Montpellier, France)p31(2003)

[35] M.Takashiri,K.Miyazaki,S.Tanaka,J.Kurosaki,D.Nagai,and H.Tsukamoto,J.Appl.Phys.,104,084302(2008).

[36] D.M.Rowe,University of Wales Cardiff,U.K.CRC Handbook of Thermoelectric (1995).

[37] L.M.Goncalves,C.Couto,P.Alpuim,A.G.Rolo,F.Volklein and J.H.Correia,Thin Solid Films.,(2009)

[38] W.Kullmann,J.Geurts,W.Richter,N.Lehner,H.Rauh,U.Steigenberger,G.Eichhorn & R.Geick,Phys.Status SolidiB.,125,131(1984).

[39] H.Zou,D.M.Rowe and G.Min,D.M.Rowe,C.Couto,J.H.Correia,Vacuum.,82 1499 (2008)

[40] D.M.Rowe and C.M.Bhandarim,Modern Thermoelectrics,Reston Publishing,Reston

(1983)

[41] L.M.Goncalves,P.Alpuim,G.Min,D.M.Rowe,C.Couto,J.H.Correia,Vacuum.,82 1499 (2008)

[42] H.Scherrer and S.Scherrer,(ch.19)CRC Handbook of Thermoelectrics.,(CRC,Boca Raton,(1995)

[43] J.R.Drabble,and C.H.L.Goodman,J.Phys.Chem.Solids.,5,142,(1958).

[44] J.O.Jenkins,J.A.Rayne and R.W.Ure,Phys.Rev.,5,3171,(1972).

[45] V.Wagner,G.Dolling,B.M.Powell and G.Landwehr,Phys.Status Solidi,85,311,(1978)

[46] M.R.Thuler,R.L.Benbow and Z.Hurych,Chem.Phys.,71,265,(1982).

[47] Caywood, L. P.;Miller, G.,"Anisotropy of the constant energy surfaces in p-type Bi_2Te_3 and Bi_2Se_3 from galvanomagnetic coefficients",Phys. Rev. B. **2** (8): 3209(1970).

[48] Satterthwaite,C. B.; Ure, R.,"Electrical and Thermal Properties of Bi2Te3".Phys. Rev. 108 (5): 1164.(1957).

[49] Tan, J.,"Proceedings of SPIE" 5836. p. 711(2005).

[50] H. J. Goldsmid, A. R. Sheard, and D. A. Wright,"The performance of Bismuth Telluride thermojunctions". Br. J. Appl. Phys. **9** (9): 365(1958).

[51] Z. Ding, S. Huang, D. Marcus, and R. Kaner,"Modification of Bismuth Telluride for Improving Thermoelectric Properties," in Thermoelectrics. Eighteenth International Conference on, pp. 721-724, 29 Aug.-2 Sept.(1999).

[52] W. Kullmann,J.Geurts,W.Richter, N.Lehner, H.Rauh,U. Steigenberger, G. Eichhorn, and R. Geick,"Effect of Hydrostatic and Uniaxial Pressure onStructural Properties and Raman Active Lattice Vibrations in Bi_2Te_3", Phys.stat.sol.(b), vol. 125, pp. 131-138.(1984).

[53] L. Caywood and G. Miller, "Anisotropy of the Constant-Energy Surfaces in N-Type Bi_2Te_3 and Bi_2Se_3 from Galvanomagnetic Coefficients," Physical Review B, vol. 2, no. 8, pp. 3209-3220,(1970).

[54] J. Jenkins, J. Rayne, and R. Ure,"Elastic Moduli and Phonon Poperties of Bi_2Te_3", Physical Review B, vol. 5, no. 8, pp. 3171-3184,(1972).

[55] J. Barnes, J. Rayne, and R. Ure,"Lattice Expansion of Bi_2Te_3 from 4.2K to 600K", Phys.Lett., vol. 46A, pp. 317-318,(1974).

[56] E. Marchenkov and V. Shipul,"Thermal Expansion of Semionductor Materials", Journal of Engineering Physics and Thermophysics, vol. 66, no. 5, pp. 547-551, (1994).

[57] J. Drabble," Progress in Semiconductors", vol. 7. John Wiley & Sons, Inc., New York,(1963).

[58] T. Harman, B. Paris, S. Miller, and H. Goering, "Preparation and Some Physical Properties of Bi_2Te_3,Sb_2Te_3 and As_2Te_3" J. Phys. Chem. Solids, vol. 2, pp. 181-190, (1957).

[59] R. Sehr and L. Testardi,"The Optical Properties of P-Type Bi_2Te_3,Sb_2Te_3 Alloys Between 2-15 Microns",J. Phys. Chem. Solids, vol. 23, pp. 1219-1224,(1962).

[60] E.Muller,W.Heiliger,P. Reinshaus and H. Submann,"Determination of the Thermal Band Gap from the Change of the Seebeck-Coefficient at the pn-Transition in $(Bi_{0.5}Sb_{0.5})_2Te_3$," in Thermoelectrics Fifteenth International Conference on, pp. 412-416,(1996).

[61] H. Kohler,"Non-Parabolicity of the Highest Valence Band of Bi_2Te_3 from Shubnikov-de Haas Effect," Phys.stat.sol.(b), vol. 74, pp. 591-600,(1976).

[62] C.Bhandari and V.Agrawal,"Thermal and Electrical Transport in Bismuth Telluride Indian Journal of Pure and Applied Physics, vol. 28, pp. 448-451,(1990).

[63] T. Scheidemantel, C. Ambrosch-Draxl, T. Thonhauser, J. Badding, and J. Sofo, "Transport Coefficients from First-Principles Calculations", Physical Review B, vol. 68, pp. 125210-1-125210-6,(2003).

[64] S. Lee and P. von Allmen,"Tight-Binding Modeling of Thermoelectric Properties of Bismuth Telluride",Appl.Phys.Lett., vol. 88, pp. 22107-1-22107-3,(2006).

[65] M. Singh and C. Bhandari, "Thermoelectric Properties of Bismuth Telluride Quantum Wires," Solid-State Comm., vol. 127, pp. 649-654, (2003).

[66] H. Scherrer and S. Scherrer, CRC Handbook of Thermoelectrics, ch. Bismuth Telluride, Antimony Telluride, and Their Solid Solutions, pp. 211-237. CRC Press, Inc.,(1994).

[67] H. Goldsmid, "The Thermal Conductivity of Bismuth Telluride," Proc. Phys. Soc. B, vol. 69, pp. 203-209,(1956).

[68] H. Goldsmid,"Heat Conduction in Bismuth Telluride", Proc. Phys. Soc., vol. 72, pp. 17-26,(1958).

[69] C.Kittel,"Introduction to Solid State Physics",7th ed.,(Wiley,New York),p.168-169,(1996).

[70] S.Iijima,"Helical Microtubules of Graphitic Carbon",Carbon Nature 354,56 (1991).

[71] C.Journet,L.Alvarez,V.Micholet,T.Guillard,M.Lamy De La Chapelle, E.Anglaret ,J.L.Sauvajol,S.Lefrant,P.Bernier,D.Laplaze,G.Flamant and A.Loiseau ,"Single Wall Carbon Nanotubes:Two Ways of production ,Syn. Met.103,2488(1999).

[72] A.Thess,R.Lee,P.Nicolaev,H.Dai ,P.Petit,J.Robert ,C.Xu,Y.H.Lee,S.G.Kim,A.G.R-inzler,D.T.Colbert,G.E.Scuseria,D.Tomanek,J.E.Fischer and R.E.Smalley, "Crystalline Ropes of Metallic Carbon Nanotubes",Science 273,483(1996).

[73] H.M.Cheng,F.Li,X.Sun,S.D.M.Brown,M.A.Pimenta,A.Marucci,G.Dresselhaus and M.S.Dresselhaus,"Bulk Morphology and Diameter Distribution Of Single-Walled Carbon Nanotubes Synthesized By Catalytic Decomposition Of Hydrocarbons",Chem.Phys.Lett.289,602(1998).

[74] Stephen Chastin,"Metal Casting: A sand casting manual for small foundary" ,Vol.II,4 ,ISBN 9780970220332.(2004)

[75] Stefanescu,Doru Michael,"Science and Engineering of Casting Solidification",2nd ed.,Springer,ISBN 9780387746098.(2008)

[76] S.Scherrer and H.Scherrer ,Citation Information,"Thermoelectric Handbook Macro to Nano",Edited by D.M. Rowe,CRC Press,Pages 27-1 to 27-19.(2006)

[77] Huaiying Zhou,Tianlong Gu,Daoguo Yang,Zhengyi Jiang,Jianmin Zeng,pages 1109-1112,"Advanced Materials Research",(Volumes 197-198).

[78] Sukhvir Singh,Rajeev Kumar and K.N.Sood,"Thin Solid Films",1078-1081.(2010)

[79] M.I.Florez-Zamora ,"Comparative Study of Al-Ni-Mo alloys obtained by mechanical alloying in different ball mills",Rev.Adv.Mater.Sci 18,301.(2008)

[80] Mechanical Alloying Technology,Institute of Materials Processing.

[81] A.Lynch and C.Rowland,"The history of grinding",SME.ISBN 0873352386.(2005)

[82] S.Bathula,M.Jayasimhadri,N.Singh,A.K.Srivastava,J.Pulikkotil,A,Dhar and R.C. Budhani,Appl.Phys.Lett.101,213902(2012).

[83] J.Schmidt,J.Koenig,A.Jacquot,H.Boettner,T.Weissgaerber,B,Kieback, " Sintering 2-Processes,Euro PM(2007).

[84] M.J.Yang,L.M.Zhang,L.Q.Han,Q.Shen and C.B.Wang,Indian J.Eng.Matter.Sci.16, 277.(2009)

[85] J.S.Son,M.K.Choi,M.K.Han,K.Park,J.Y.Kim,S.J.Lim,M.Oh,Y.Kuk,C.Park,S.J.Kim and T.Hyeon,Nano Lett.12,640.(2012)

[86] J.D.Boor and V.Schmidt,Adv.Matter.22,4303.(2010)

[87] A.W.Hull,J.Am.Chem.Soc.41(8),1168.(1919)

[88] B.D.Cullity,Addison –Wesley Series in Metallurgy and Materials.(1978)

[89] R.J.Keyes,A.J.Garrett-Reed,P.J.Goodhew and G.Lorimer,"Introduction to Scanning Transmission Electron Microscopy",Bios,Oxford.(1998)

[90] M.K.Miller,"Atom Probe Tomography",Kluwer,Dordrecht.(2000)

[91] M.Prutton,"Introduction to Surface Physics",Oxford University Press,Oxford.(1994)

[92] L.Reimer,"Scanning Electron Microscopy",Springer,Berlin.(1995)

[93] C.J.R.Sheppard and D.M.Shotton,"Confocal Laser Scanning Microscopy",Bios,Oxford.(1997)

[94] L.Solymar and D.Walsh,"Lectures on the Electrical Properties of Materials",Oxford University Press.(1995)

[95] J.Stohr,NEXAFS Spectroscopy,Springer-Verlag,Berlin(1992)

[96] J.F.Watts,"Introduction to Surface Analysis by XPS and AES",John Wiley &Sons Ltd. Chichester.(2003)

[97] X.B.Zhao,H.Ji,Y.H.Zhang,T.J.Zhu,J.P.Tu and X.B.Zhang,APL 86,062111.(2005)

[98] G.Yun,L.L.Yun,T.P.Heng,L.L.Qi and Z.Zhong,Chinese Sci.Bull.,55,3978.(2010)

[99] N.Pierard,A.Fonseca,J.F.Colomer,C.Bossuot,J.M.Benoit,G.VanTendeloo,J.P.Pirard and J.B. Nagy,"Ball milling effect on the structure of single-wall carbon nanotubes",Science Direct.(2004)

[100] B. D. Cullity ,"Addison-Wesley Series in Metallurgy and Materials."(1978).

[101] W.J. Parker, W.J.Jenkins,C.P.Butler and G.L.Abbott,J.App.Phys.32,(9),1679 (1961).